



Characteristics and formation mechanism of mesogenetic dissolution: A case study of Ordovician carbonate in the western slope of the Shulu Sag, Jizhong Depression, Bohai Bay Basin

Pengfei Xiang^{a,b}, Hancheng Ji^{a,b,*}, Yanqing Shi^{a,b}, Yebo Du^c, Peng Chen^{a,b}, Qingping Weng^{a,b}, Xinrong Xu^{a,b}, Yushu Sun^{a,b}, Yun Huang^d, Shuqi Zou^{a,b}

^a State Key Laboratory of Petroleum Resources and Prospecting, China University of Petroleum (Beijing), Beijing, 102249, China

^b College of Geosciences, China University of Petroleum, Beijing, 102249, China

^c Research Institute of Petroleum Exploration Development, Beijing, 100034, China

^d Exploration and Development Research Institute of Huabei Oilfield Company, Hebei Renqiu, 062552, China

ARTICLE INFO

Keywords:

Mesogenetic dissolution
Shulu Sag
Ordovician carbonate reservoir
Formation mechanism

ABSTRACT

Mesogenetic dissolution has the potential to enhance the quality of carbonate reservoirs, and thus it is critical to identify the source of corrosive fluids and establish the mechanism that leads to mesogenetic dissolution. An integrated study using cores, thin sections, seismic profiles, and geochemistry was performed to investigate the characteristics, discuss the possible corrosive fluids, and establish the formation mechanism of mesogenetic dissolution in Ordovician carbonates in the western slope of the Shulu Sag, Bohai Bay Basin. The Shulu Sag underwent a four-stage growth history, and the carbonate rocks in the study area experienced three episodes of diagenetic alteration (i.e., syngenetic, telogenetic, and mesogenetic). The micro- and macroscopic occurrences of mesogenetic dissolution were ubiquitous, including, for example, stylolites, solution seams, tiny pores, laminar dissolution pores, dissolution pores and vugs associated with stylolites, dissolution enlarged fractures, erosion of late minerals (e.g., saddle dolomite), and related hydrocarbon inclusions. The partition patterns of trace elements normalized to Upper Crust Continent (UCC) and rare earth elements (REEs) normalized to Post-Archean Australian Shale (PAAS) were consistent between eroded and uneroded samples. Compared with uneroded samples, eroded samples had higher contents of some trace elements (e.g., Co, Cr, Cu, Ni, V, and Zn) and REEs, and relatively higher average $\delta^{13}\text{C}$ values and $^{87}\text{Sr}/^{86}\text{Sr}$ ratios. These characteristics indicate that the most likely corrosive fluids causing dissolution were organic acids in hydrocarbon-bearing fluids, which may have been derived from the maturation of organic matter in marlstone in the lower part of the Sha3 member (Es_3^1). The combination of the tilted basin structure and presence of good conduits (i.e., unconformity, stylolites, and fractures) promoted the migration of corrosive fluids and the occurrence of mesogenetic dissolution in Ordovician reservoirs from the Neogene-Quaternary period to the present. A geologic model for the formation mechanism of mesogenetic dissolution has been proposed, which provides new insight for future hydrocarbon exploration.

1. Introduction

Carbonate rocks account for 20% of the total sedimentary rocks worldwide, which contain as much as 50–60% of the world's oil and gas reserves (Morse and Mackenzie, 1990; Burchette, 2012). It is of considerable significance to study the formation and evolution of pores in such reservoirs. In general, the primary porosity of newly deposited carbonate ooze and mixed sediments varies from 60% to 80% (Garrison,

1981; Fabricius, 2003). Most primary pores, except in the early hydrocarbon filling, are usually compressed by compaction and cementation during post-depositional burial resulting in the preservation of less primary porosity (Halley and Schmoker, 1983; Goldhammer, 1997). As one of the main diagenetic processes leading to secondary pore formation, dissolution in carbonate rocks usually improves reservoir quality to varying degrees (Moore and Wade, 2013). Carbonate dissolution can be divided into eogenetic, mesogenetic, and telogenetic dissolution based

* Corresponding author. China University of Petroleum-Beijing, 18 Fuxue Road, Changping, Beijing, 102249, China.

E-mail address: jhch@cup.edu.cn (H. Ji).

<https://doi.org/10.1016/j.petrol.2021.109045>

Received 16 November 2020; Received in revised form 29 March 2021; Accepted 29 May 2021

Available online 8 June 2021

0920-4105/© 2021 Elsevier B.V. All rights reserved.

on different time-porosity formation regimes (Choquette and Pray, 1970). Most carbonate minerals are undersaturated in meteoric water, which leads to an increase in porosity by dissolution (e.g., Longman, 1980; James and Choquette, 1984; Mazzullo, 2004; Mazzullo and Harris, 1991; Moore and Wade, 2013). Therefore, there is widespread agreement that good porosity is easily generated in the telogenetic or eogenetic systems resulting from meteoric water leaching (e.g., Vacher and Mylroie, 2002). With respect to mesogenetic dissolution, which is also referred to as “deep karst” (e.g., Jia and Hao, 1989; Sauro et al., 2013), “burial dissolution” (e.g., Lambert et al., 2006; Zhu et al., 2007; Liu et al., 2008), or “deep burial dissolution” (e.g., Xu et al., 2017; Valencia and Laya, 2020), there has been ongoing debate as to whether it can generate valid porosity. Since the 1980s, the burial environment and related diagenetic processes (e.g., mesogenetic dissolution) have gradually received increasing attention from scientists (e.g., Moore and Druckman, 1981; Mazzullo and Harris, 1991, 1992; Zhu et al., 2007; Liu et al., 2008; Jin et al., 2009; Jiang et al., 2015; Jia et al., 2016; Bai et al., 2020). Some geologists have demonstrated the significance of mesogenetic dissolution in increasing the porosity of carbonate rocks, although cementation, and mechanical and chemical compaction can result in porosity loss under deep-burial conditions (Wierzbicki et al., 2006; Barnett et al., 2015; Valencia and Laya, 2020). In particular, Mazzullo and Harris (1992) provided a detailed review of the characteristics of mesogenetic dissolution in carbonate rocks (e.g., pore types and evolution, and fluids causing mesogenetic dissolution). Ehrenberg et al. (2012), however, disputed the mesogenetic dissolution model due to a lack of supporting empirical data and the violation of chemical constraints on mass transport. In China though, widespread development of burial (mesogenetic) dissolution has been demonstrated, for example, in the Tarim Basin (e.g., Zhu et al., 2007; Liu et al., 2008; Jin et al., 2009; Jia et al., 2016; Bai et al., 2020), Sichuan Basin (e.g., Hao et al., 2015; Hu et al., 2020), Ordos Basin (e.g., Tan et al., 2017), Bohai Bay Basin (e.g., Zhao et al., 2016; Xu et al., 2017), Qaidam Basin (e.g., Feng et al., 2013), and Pearl River Mouth Basin (Jiang et al., 2015).

These case examples provide indisputable evidence that mesogenetic dissolution has a significant effect on the formation of high-quality reservoirs.

Hydrocarbon exploration in the Shulu Sag, one of the most significant petroliferous basins in the Huabei oilfield, has mainly focused on Cenozoic clastic rock and carbonate burial-hill top reservoirs and has been ongoing since the late 1970s. From 2016 until now, wells drilled into Ordovician strata along the western slope zone have shown great potential. Due to tectonic uplift, most geologists have argued that early meteoric freshwater dissolution resulted in the generation of all porosity in the reservoirs (e.g., Li, 2013). However, we have found that a portion of the storage space in the carbonate rocks did not generate under subaerial conditions but rather within the mesogenetic environment. Therefore, the primary goals of this study were to answer the following questions by conducting an integrated study of petrography and geochemistry on samples from the Ordovician strata:

- (1) What are the detailed characteristics of diagenesis corresponding to mesogenetic dissolution in Ordovician carbonate rocks?
- (2) What are the associated fluids that most likely caused dissolution in the mesogenetic realm?
- (3) What is the formation mechanism of mesogenetic dissolution and the influence of mesogenetic dissolution on reservoirs?

2. Geological setting

The Bohai Bay Basin is a NE-SW trending, rhomb-shaped strike-slip pull-apart basin (Fig. 1A), which developed from the Late Mesozoic to Early Cenozoic by lithospheric extension and thermal subsidence from the India-Eurasia collision (Hou et al., 1998; Li et al., 2010), and includes a series of uplifts and depressions, such as the Jizhong Depression (Fig. 1A). The Shulu Sag, located in the southwestern corner of the Jizhong Depression (Fig. 1A), is a typical elongated half-graben basin covering about 700 km² bounded to the southeast by the Xinhe Uplift

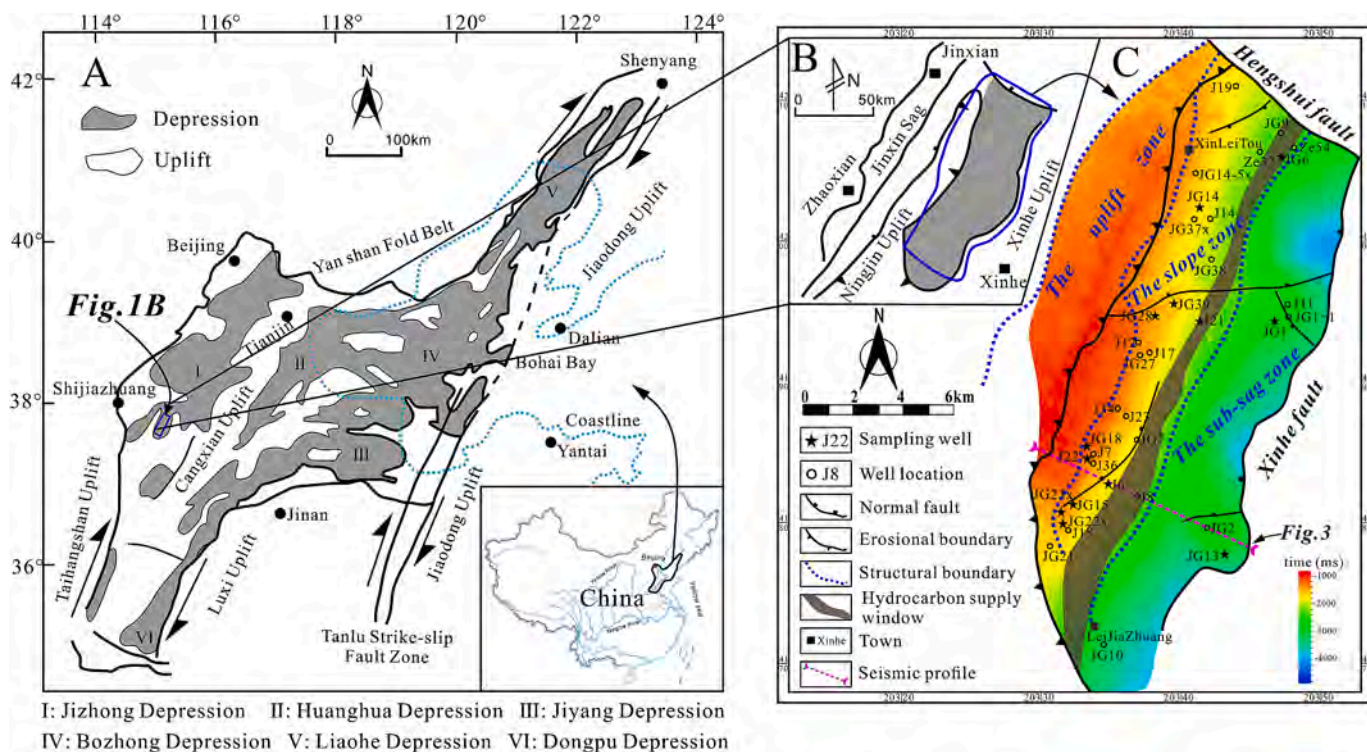


Fig. 1. (A) Locations of the Bohai Bay Basin and the Shulu Sag (modified after Jiang et al., 2007). (B) The structure features of the Shulu Sag. (C) Comprehensive diagram showing well locations in the western slope of the Shulu Sag, the time-domain map of the Tg2 seismic reflection horizon (see in Figs. 2 and 3), and the hydrocarbon supply window (from Cai et al., 2020).

and to the west by the Ningjing Uplift (Zhao et al., 2014; Ren et al., 2019, Fig. 1B). The Shulu Sag is typically classified into three tectonic units based on the tectonic subsidence history from west to east: the western gentle slope zone, the central sub-sag zone, and the eastern steep slope zone (Zhao et al., 2014). The western gentle slope zone, which is the current study area owing to its exploration potential, has an area of about 370 km² with a length and width of about 43 km and 10 km, respectively (Ren et al., 2019, Fig. 1C). Tectonic events in the Jizhong Depression control the development and structural evolution of the Shulu Sag.

The eastward-dipping, tilted block forms the bedrock of the Shulu Sag, which consists of Archean-Palaeoproterozoic metamorphic rocks, and Meso-Neoproterozoic through Palaeozoic deposits that include Cambro-Ordovician and Permo-Carboniferous strata (Jiang et al., 2007), but lacks the Silurian and Devonian sedimentary succession as a result of Late Caledonian-Hercynian tectonic uplift (Fig. 2). The Permo-Carboniferous strata, which have only been preserved in the basin center, are composed of alternating marine and continental coal-bearing series (Lao and Gao, 1984, Figs. 2 and 3). Therefore, they are directly overlain by Eocene to Pliocene lacustrine sediments. The Lower Cambrian sediments (C_{1m}, C_{1mz}) are dominated by siliciclastics intercalated with carbonates deposited during the platform foundation, while the Middle (C_{2x}, C_{2z}) and Upper Cambrian successions (C_{3g}, C_{3c}, C_{3f}) were deposited on oolite- and storm-dominated carbonate ramp systems, respectively (An et al., 1982; Chen and Meng, 1993; Meng et al., 1997, Fig. 2). However, the upper Cambrian through Ordovician strata are dominated by fine-grained limestones and dolostones that were deposited on a low-energy, epeiric-sea carbonate platform (An et al., 1982; Feng et al., 1989; Chen and Meng, 1993; Meng et al., 1997). This study focuses on the Ordovician strata composed of the Yeli (O_{1y}), Liangjiashan (O_{1l}), Majiagou (O_{2m}), and Fengfeng (O_{2f}) Formations in ascending order in the western gentle slope zone (Figs. 1C and 2). The lacustrine basin fill materials gradually overlap upward onto the Ordovician strata at the western slope of the Shulu Sag (Fig. 3). These are mainly composed of terrestrial deposits, such as mudstones, sandstones, and conglomerates, including the Shahejie (Es), Dongying (Ed), Guantao, Minghuazhen, and Pingyuan Formations from bottom to top in the basin depocenter (Fig. 2). It is worth mentioning that the Shahejie Formation comprises three members: Sha1 (Es₁), Sha2 (Es₂), and Sha3 (Es₃, including upper and lower parts) (Fig. 2). The lower part of the Sha3 member (Es₃¹) is composed of organic matter-rich marlstones intercalated with mudstones that act as the primary source rocks (thickness 400–600 m) for the Shulu Sag (Liang et al., 2001; Zhao et al., 2014; Zou et al., 2015; Huo et al., 2019; Ren et al., 2019; Cai et al., 2020; Kong et al., 2020).

3. Samples and methods

A total of 27 wells were drilled into Ordovician strata, 74 core samples were randomly collected from Ordovician strata in 18 wells, and 3D seismic data for the western slope of the Shulu Sag were obtained from the Huabei Oilfield Branch Company (CNPC). Seismic profiles from 3D seismic data were first used to realize the characteristics of stratigraphic and structural distribution and then to establish the tectonic evolution process. All rock samples were made into doubly polished casting thin sections, which were half-stained with alizarin red-S solution to differentiate dolomite from calcite (Friedman, 1959), and impregnated with blue-epoxy to identify reservoir storage space. The investigation of petrographic and diagenetic features was based on standard transmitted-light microscopy (plain and polarized light). Cathodoluminescence (CL) analysis was performed on 21 samples, to obtain visual information on the distribution of trace elements in minerals, especially manganese (Mg²⁺) and iron (Fe²⁺) ions (Machel and Burton, 1991; Scholle and Ulmer-Scholle, 2003). Fluid inclusion microthermometry was undertaken on calcite precipitated in fractures and pores in seven samples. All analyses mentioned above were

performed at the State Key Laboratory of Petroleum Resources and Prospecting, China University of Petroleum (Beijing).

In addition, 36 fresh bulk samples were chosen and ground to powder (<200 mesh) for carbon (δ¹³C) and oxygen (δ¹⁸O) isotope examination, and of these, 20 samples were also analyzed for strontium isotopes, and 27 samples for trace elements and rare earth elements (REEs). The elemental and isotopic analyses were carried out on both eroded and uneroded parts of samples using a micro-drilling method to investigate the influence of fluids likely causing mesogenetic dissolution, in accordance with the methods of Liu et al. (2008) and Jin et al. (2009). Analyses for carbon and oxygen isotopes, strontium isotopes, and trace metals and REEs were carried out at the State Key Laboratory of Petroleum Resources and Prospecting of China University of Petroleum (Beijing), the Institute of Geology and Geophysics of the Chinese Academy of Sciences (IGGCAS), and the Analytical Laboratory of the Beijing Research Institute of Uranium Geology (ALBRIUG), respectively.

Analytical equipment, operational procedures, and corresponding experimental principles for the analyses mentioned above have been described in detail by Xiang et al. (2020) with the exception of fluid inclusion microthermometry analysis, which is detailed in Liu et al. (2017).

4. Results

4.1. Basin tectonic evolution from the Ordovician to the present

The development of the Shulu Sag is intrinsically connected to the tectonic evolution of the Jizhong Depression. Based on the synthesis of stratigraphy and basin architecture, the tectonic evolution of the Shulu Sag was defined as having a four-stage growth history from the Ordovician to the present, as illustrated with 2D MOVE software using the southern seismic profile of the study area as an example (Figs. 3 and 4). In stage 1, after the late Ordovician was deposited, pre-existing sediments underwent regional tectonic uplift and a long period of denudation lasting until the early Carboniferous that resulted from Caledonian and Hercynian movements (Fig. 2). Thus, there was no deposition in the Devonian, Silurian, and even the upper part of the Ordovician strata as they were entirely eroded, which led to a vital regional-unconformity surface in the Jizhong Depression (Figs. 2 and 4). Subsequently, the unconformity was covered by Carboniferous-Permian sediments (Fig. 4b). In stage 2, the Indosinian-Yanshanian orogenies caused the fold deformation of pre-existing strata, high-angle fractures, and a lack of deposition during the Mesozoic (Fig. 2). In stage 3, the evolution of a boundary fault (i.e., Xinhe fault) made the Shulu area, as a rift lake basin, experience terrestrial fillings whose provenance supply was from the western tilted carbonate successions during the early Eocene to late Paleogene (i.e., syn rifting stage) (Figs. 2 and 4c–g). The Ordovician strata in the study area were gradually buried by overlying sediments. In stage 4, the Shulu Sag was mainly subjected to thermal subsidence (i.e., post rifting) and received Neogene to Quaternary terrestrial deposits from the late Paleogene to present-day (Figs. 2 and 4h).

4.2. Diagenesis

Based on the petrographic features of diagenesis and tectonic evolution, integrated with the burial history, the carbonate rocks of the Ordovician Formation in the western slope of the Shulu Sag were mainly altered by twelve diagenetic events that occurred over three different diagenetic stages (Figs. 5–7). These stages consist of the syngenetic, telogenetic, and mesogenetic, corresponding to marine, meteoric water, and burial environments, respectively. A detailed paragenesis is depicted in Fig. 5, and brief descriptions of the three diagenetic stages are provided below.

4.2.1. Stage 1: syngenetic diagenesis

This stage is a combination of diagenetic modification by early weak

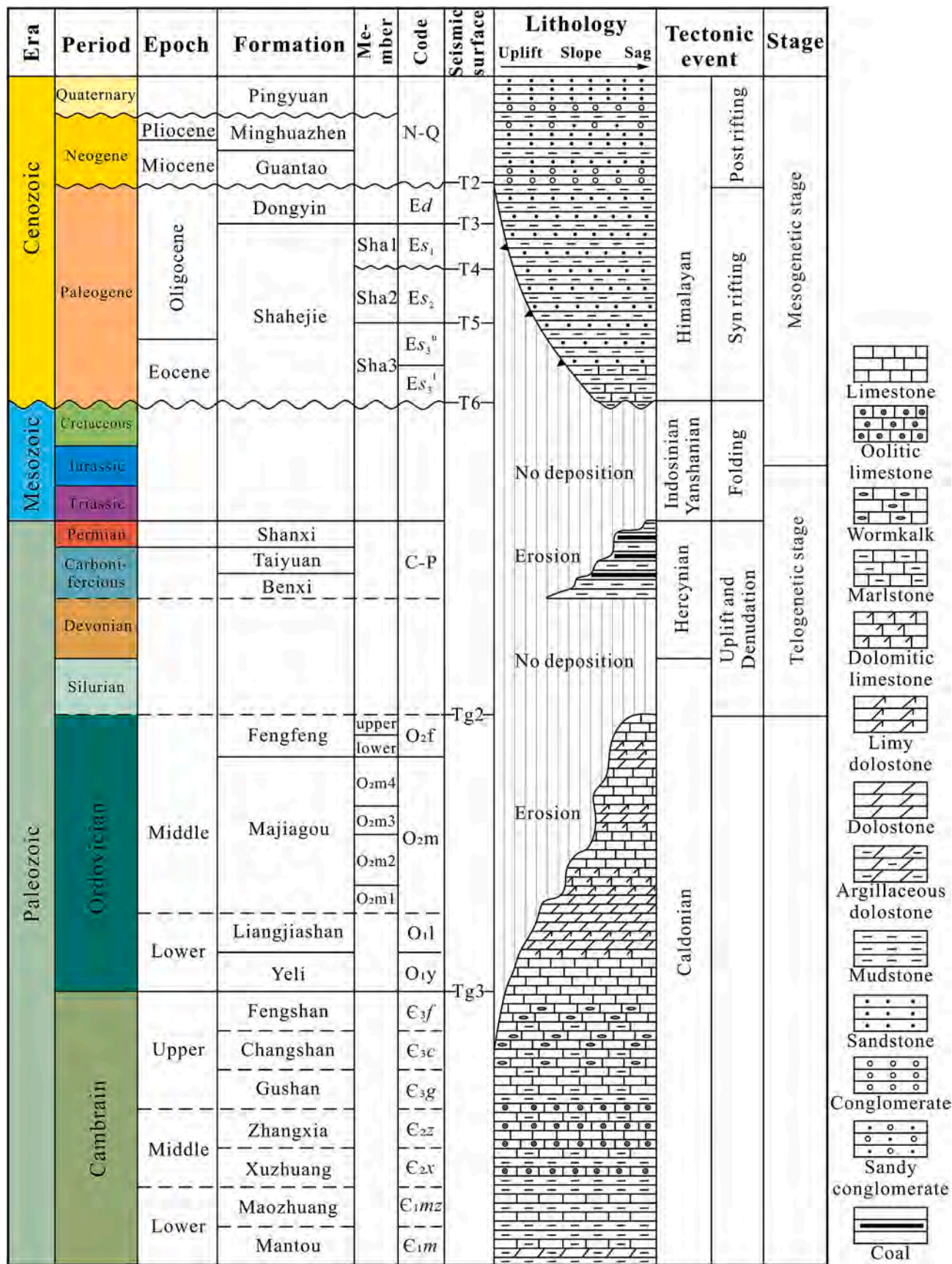


Fig. 2. Comprehensive stratigraphic column of the Shulu Sag. This column also shows corresponding tectonic events at different stages in Fig. 4.

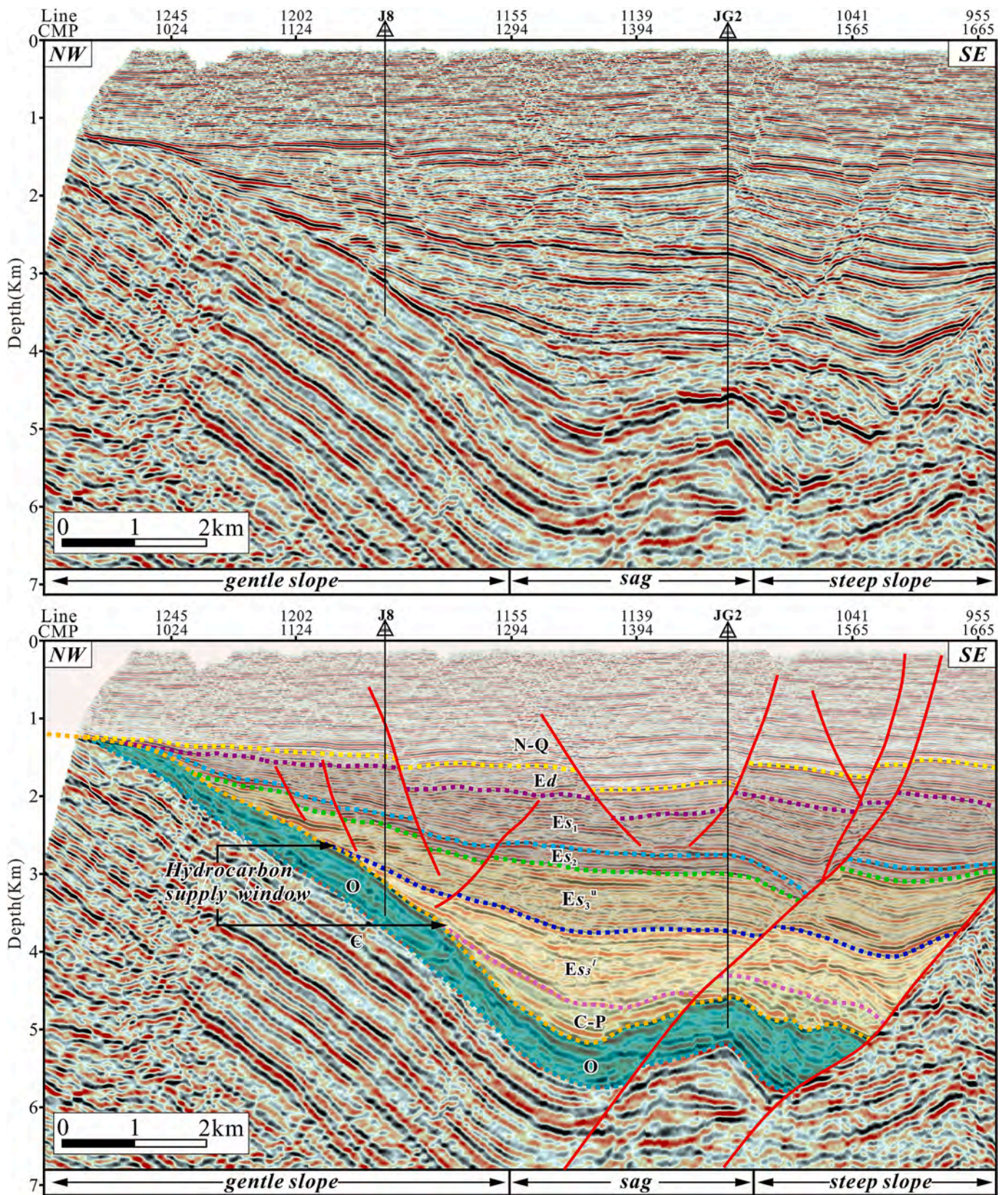


Fig. 3. Uninterpreted and interpreted seismic-reflection profile across the southern of the Shulu Sag. The location of the seismic profile is shown in Fig. 1C, and the dashed lines with different colors represent different seismic-reflection boundaries displayed in Fig. 4.

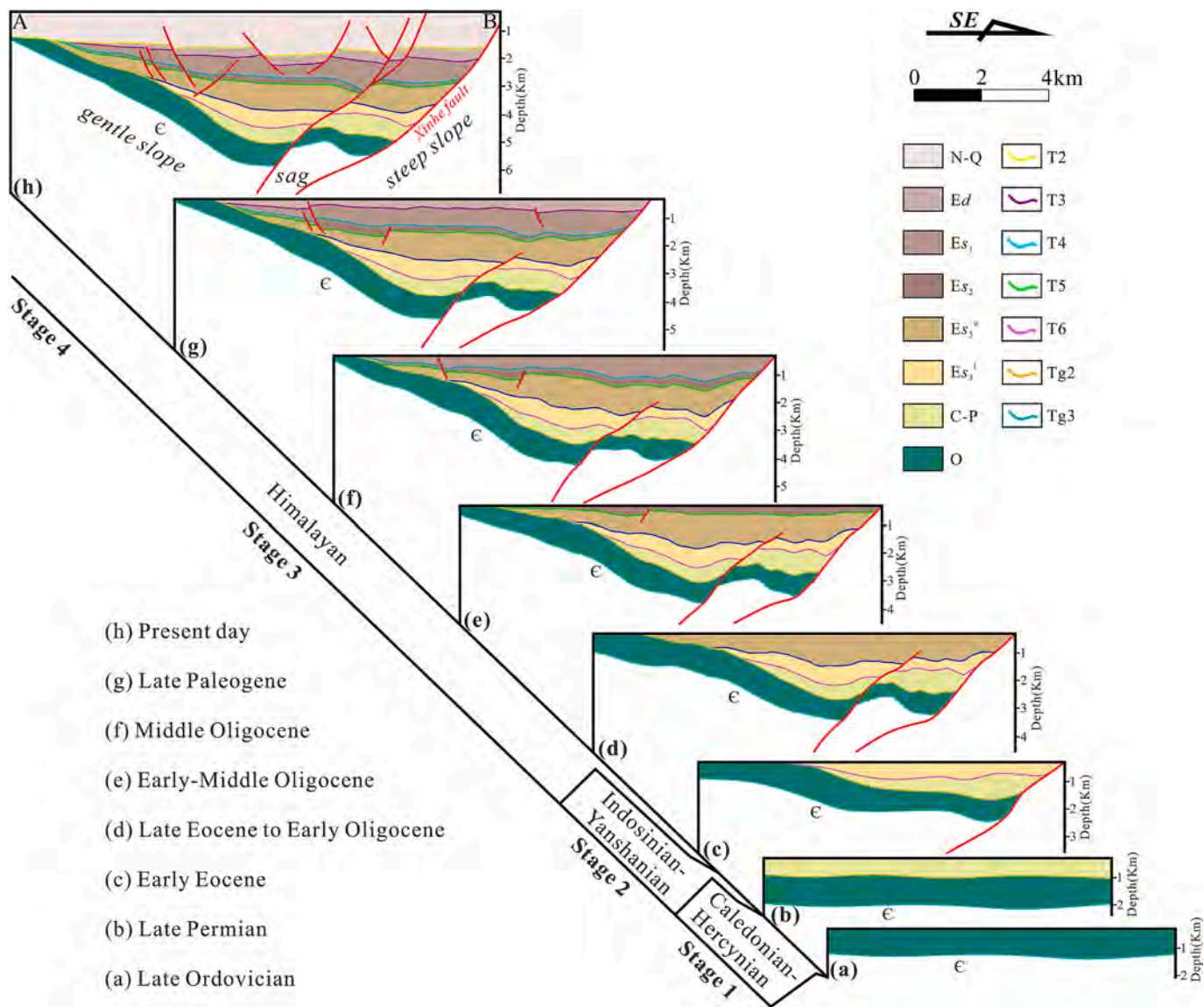


Fig. 4. Schematic diagram illustrating the tectonic evolution of the Shulu Sag from Ordovician to present day. The seismic profile is shown in Fig. 3, whose location is displayed in Fig. 1C.

mechanical-compaction, calcite cementation, and dolomitization that occurred in the marine environment (Fig. 5). The isopachous fibrous to bladed high-Mg calcite cement usually occurred around intraclasts or grains (Fig. 6A, B), which is a typical feature of penecontemporaneous marine cement as the first calcite generation linked with seawater (Scholle and Ulmer-Scholle, 2003), and displayed non-luminescence under CL (Fig. 7H). Dolomites had a similar luminescence color with micrites, i.e., a dull red color (Fig. 7A, B), indicating an oxidizing environment, which might represent a penecontemporaneous sabkha-type origin formed in supratidal flats (Feng and Jin, 1994). Silty-fine crystalline dolomite was typically characterized by crystals with a dirty core and clear rim that, respectively, appeared as dull red and bright red under CL (Fig. 7C), which probably suggests a seep-reflux dolomitization origin during the penecontemporaneous or post-penecontemporaneous period in a suboxic environment (Feng and Jin, 1994).

4.2.2. Stage 2: telogenetic diagenesis

According to the tectonic evolutionary history of the Shulu Sag (Fig. 4), the Ordovician strata were uplifted as a whole, after the Fengfeng Formation was deposited, i.e., from the late Caledonian to

Hercynian (Meng et al., 1997, Figs. 2 and 5). The upper Ordovician unit was exposed to subaerial conditions and became a weathered crust due to a prolonged period of meteoric water leaching and erosion. Thus, this stage was dominated by calcite cement and extensive dissolution features distributed in meteoric freshwater areas, e.g., sinkholes, caves, and vugs (Fig. 6F), karstification, and brecciation (Figs. 5 and 6D, E). Macroscopic characteristics of the palaeokarst were identified from cores, including the unconformity surface (Fig. 3), breccia deposits, oxidized colors, and weathering clay. Thus, some fracture-vug systems were formed during this stage. Vugs were typically up to several centimeters in size with different irregular shapes. Fractures in the cores were commonly 2–8 mm in width with smooth borders, and principally included tectoclasses and weathering fissures. Most of these storage spaces were cemented by blocky or granular calcites that exhibit non- or dull luminescence because meteoric water in the telogenetic realm is oxidizing, which generally results in low Fe²⁺ and Mn²⁺ contents in pore waters (Scholle and Ulmer-Scholle, 2003). Meanwhile, some coarse blocky calcite cements exhibited alternating bright orange and non-luminescence in strong oscillatory zonal growth (Fig. 7E), which indicates a probable fluctuation in redox conditions within an extensively fractured-cavitated rock that underwent an alteration beneath

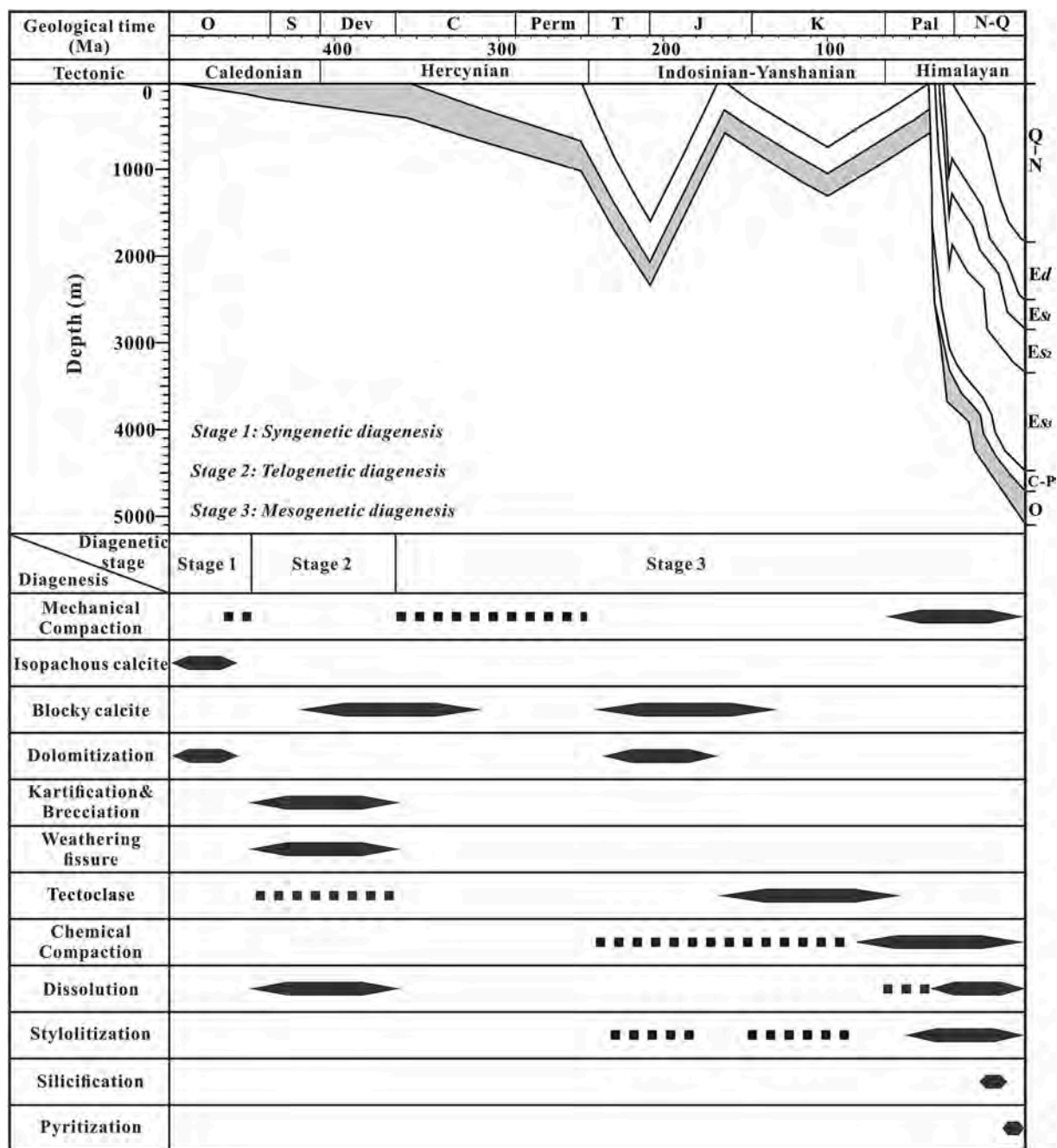


Fig. 5. Diagram illustrating diagenetic paragenesis and burial history of the Ordovician carbonates in the study area.

multiple subaerial exposure surfaces.

4.2.3. Stage 3: mesogenetic diagenesis

This stage is mainly characterized by a mix of strong mechanical and chemical compaction, calcite cementation, burial dolomitization, and related mesogenetic dissolution (Fig. 5). The presence of broken and deformed grains or intraclasts demonstrates intense mechanical compaction in a deep burial environment (Fig. 6A, B). Widely distributed pressure solution structures provided evidence of chemical compaction in cores and thin sections, including stylolites (Fig. 6G, I), wispy microstylolites (Fig. 6H), and solution seams (Fig. 6H). Blocky poikilotopic calcite cement with elevated Fe²⁺ and Mn²⁺ contents in a reducing environment exhibited bright orange luminescence in the fractures (Fig. 7F) or a transition from a bright to dull luminescence response in the fracture-vugs (Fig. 7G, H). The latter might be

interpreted as a transition from having enough Fe²⁺ and Mn²⁺ incorporation to a condition in which availability and incorporation of Fe²⁺ exceeds that of Mn²⁺ under reducing conditions. Many of these calcites were strongly twinned, reflecting stresses on the calcite lattice generated by nearby faults (Fig. 6C). The homogenization temperatures of primary two-phase fluid inclusions in these blocky calcites (Fig. 8) that filled in fractures and vugs varied from 137.5 °C to 177.3 °C with an average value of 165.7 °C (Table S1). Furthermore, 80% of these temperatures were higher than 160 °C (Fig. 9), which also supports a burial environment as the origin. In the mesogenetic realm, the partial matrix of rock was completely dolomitized by marine-related fluids as evidenced by the dull red luminescence, to form fine-coarse subhedral to anhedral crystalline dolomites (100–250 μm) (Fig. 7D). In addition, euhedral dolomite crystals were dispersedly distributed along or in the shadow of stylolites (Fig. 6J), and formed from Mg²⁺-rich fluid that migrated along

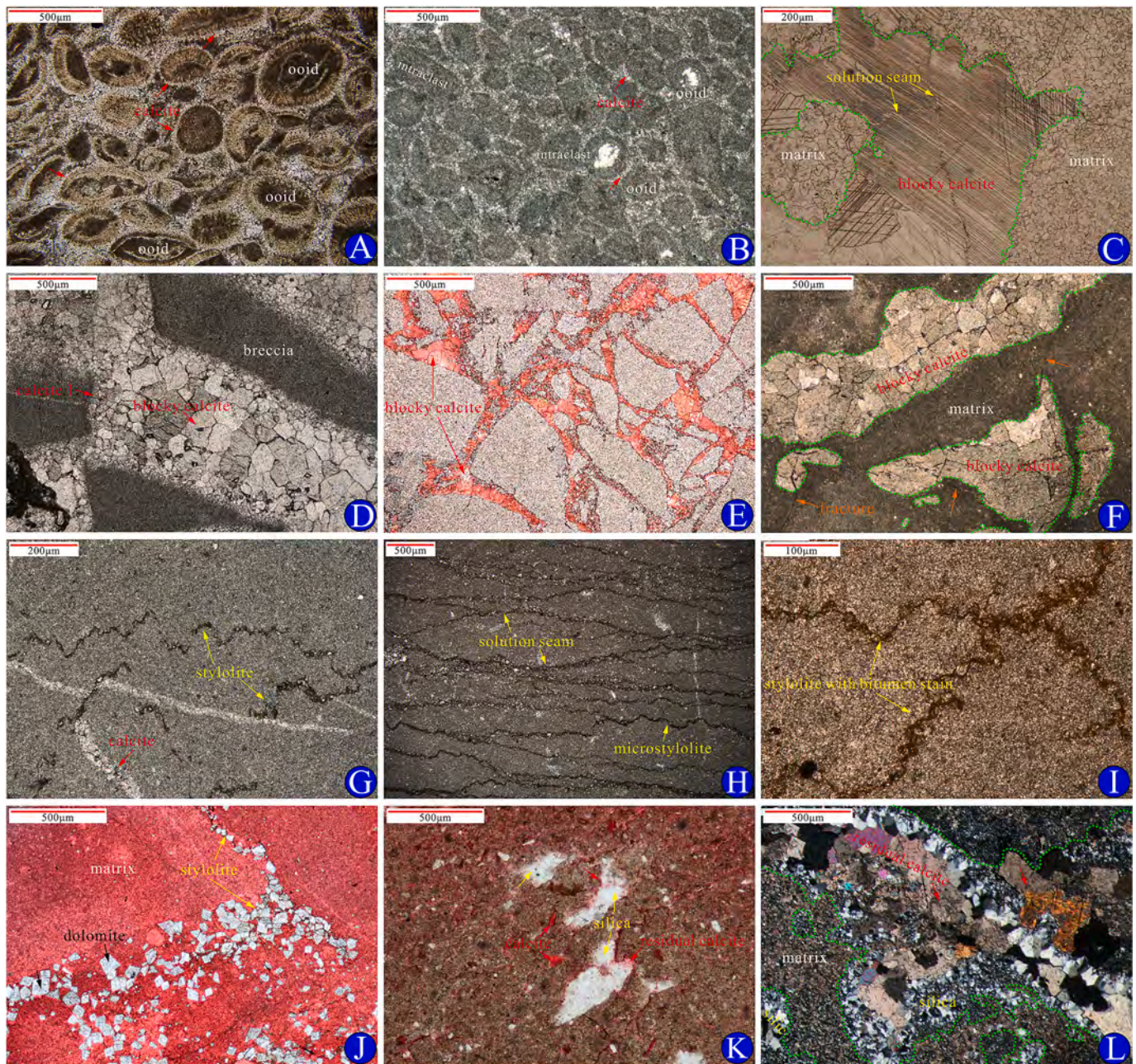


Fig. 6. Microphotographs of thin section observations (PPL-plane-polarized light; XPL-cross-polarized light). (A) Oolitic limestone with features of broken or deformed ooids cemented by early isopachous fibrous marine calcite cement, well JG28x, 1719.44 m, O₂m2, PPL. (B) Grainstone with early isopachous fibrous calcite cement; grains include ooids and intraclasts, well J6, 2580.00 m, O₂m2, PPL. (C) Silty crystalline limestone, vug-filling blocky calcite with late solution seams, well JG1, 4058.58 m, O₂f, PPL. (D) Brecciated micrite with intergranular space cemented by two phases calcite, well J22, 1346.00 m, O₂m3, PPL. (E) Brecciated dolomitic micrite with blocky calcites fills between breccias, well JG15, 1582.90 m, O₂m4, PPL. (F) Micrite with vugs filled by blocky calcites, well J22, 1355.40 m, O₂m3, PPL. (G) Micrite, stylolites cut the previous calcite filled in fracture, well J22, 1347.07 m, O₂m3, PPL. (H) Micrite with numerous solution seams and microstylolites, well J22, 1393.05 m, O₂m2, PPL. (I) Micrite with two stylolites charged of bitumen, well J22, 1393.00 m, O₂m3, PPL. (J) Micrite with dolomite crystals developed in and along the stylolites, well J6, 2573.00 m, O₂m2, PPL. (K) Marlstone with dissolution pores filled by calcites, which then are replaced by silica, well JG6, 3463.00 m, O₂f, PPL. (L) Previous calcites cemented in vugs of micrite are incompletely replaced by silica, well JG39, 2003.60 m, O₂m2, XPL.

stylolites. Saddle dolomites present in vugs were dissolved by aggressive fluids, which is another typical characteristic of burial dolomitization (Davies and Smith, 2006). Some of the cement that previously filled in the vugs or fractures was imperfectly replaced by silica, forming a sharp boundary with the surrounding matrix in the form of chalcedony or micro-quartz (Fig. 6K, L). At the same time, metal sulphides were present in the form of pyrites, occurring as either individual crystals (~300 μm) or clusters of crystals (~1 cm), and were commonly observed to partially or entirely replace cement fillings in pores or vugs (Figs. 10E, F

and 11N) and distribute along the boundary of fractures (Fig. 11O). A detailed description of the characteristics of mesogenetic dissolution is presented in the next section.

4.3. Petrographic characteristics of mesogenetic dissolution

Detailed core and thin-section observations demonstrate that the pores in the study area are almost wholly secondary in origin. Most of the pores were caused by mesogenetic dissolution, which was widely

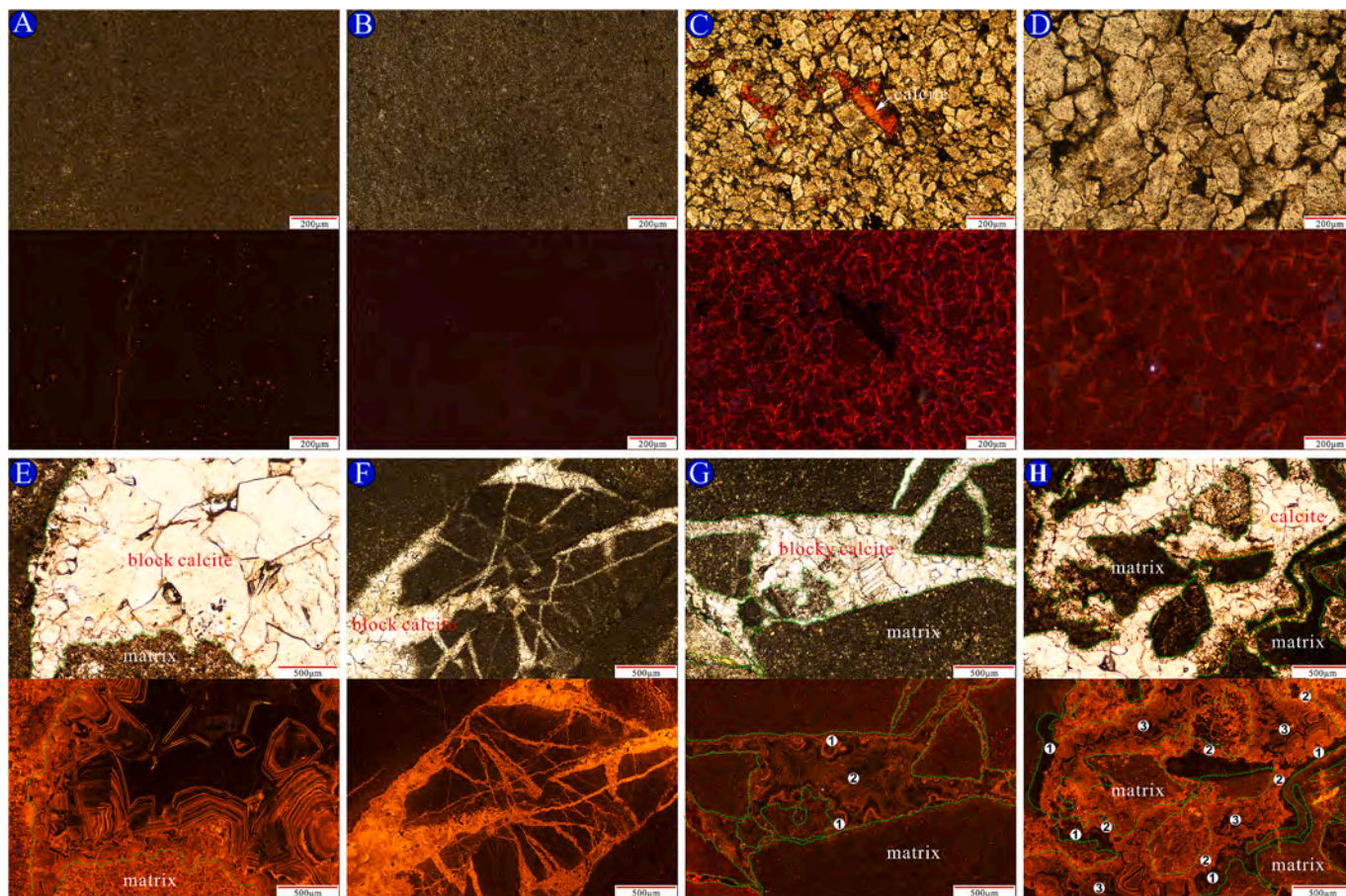


Fig. 7. Microphotographs under plane-polarized light (upper) and cathodoluminescence (CL) (lower) displaying the diagenetic features. (A) Micrite with non-luminescence, well J22, 1404.00 m, O₂m2. (B) Dolomicrite with dull to dull-red luminescence, well J22, 1357.55 m, O₂m3. (C) Silty-fine crystalline dolomite characterized by a dirty core with a clean rim showing dull red and bright red under CL, well J6, 2583.40 m, O₂m2. (D) Coarse crystalline dolomite showing the same luminescence with silty-fine crystals, well JG14, 2424.80 m, O₂m2. (E) Coarse blocky calcites filled in vug showing alternating bright orange and non-luminescence in strong oscillatory zonal growth, which postdates other calcites, well J22, 1351.17 m, O₂m3. (F) Micrite with fractures filled by calcites showing bright orange luminescence, well J22, 1411.20 m, O₂m2. (G) Brecciated micrite, intergranular space filled by calcites with oscillatory zonal growth, showing alternating dull orange and non-luminescence, well J21, 2719.08 m, O₂m4. (H) Brecciated micrite, space precipitated by three generation calcites, including ① non-luminescence, ② bright orange, and ③ oscillatory zonal growth alternating bright orange and non-luminescence, respectively, well J22, 1351.17 m, O₂m3.

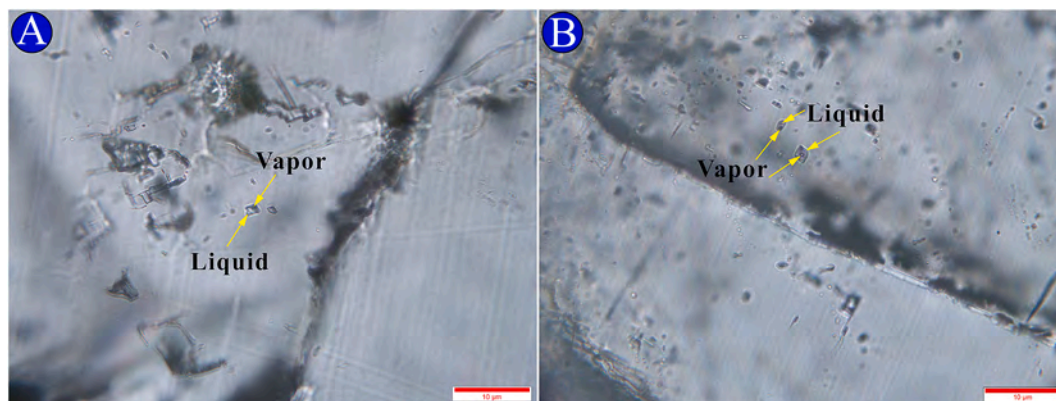


Fig. 8. Photomicrographs showing two-phase (L + V) aqueous inclusions in the blocky calcite cement, “L” standing for liquid phase, “V” for vapor phase. (A) Well J22, 1397.80m, O₂m2. (B) Well JG13, 4986.65m, O₂f.

observed in the Ordovician limestone or dolostone. In accordance with the general criteria of mesogenetic dissolution identification from [Mazzullo and Harris \(1992\)](#), evidence of mesogenetic dissolution includes (1) stylolites, (2) tiny pores and vugs associated with stylolites, (3) dissolution-enlarged fractures, (4) corrosion of late minerals, such as

poikilotopic calcite and saddle dolomite, and (5) the occurrence of bitumen in secondary pores.

4.3.1. Stylolites and related hydrocarbon inclusions

As direct discriminatory evidence of the mesogenetic environment,

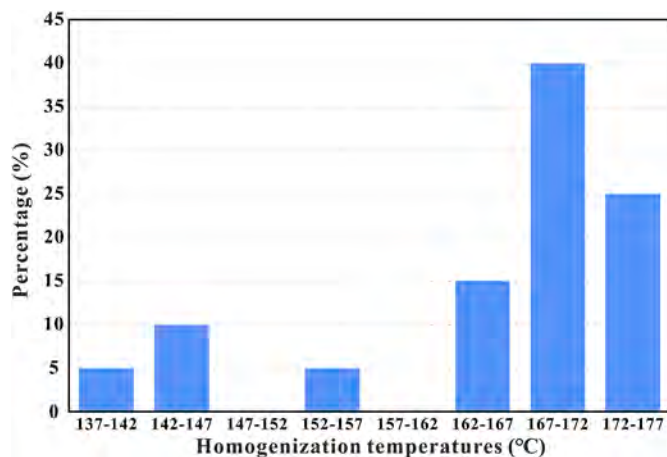


Fig. 9. Histograms showing homogenization temperatures measured from two-phase aqueous inclusions of blocky calcites from the Ordovician carbonates in wells J22 and JG13.

stylolites were most abundant in the Ordovician strata, including wavy (Figs. 6G and 11H), jagged stylolites (Figs. 6I and 10B), and wispy seams (Figs. 6H and 10A, C) triggered by chemical pressure-dissolution effects resulting from an increase in overburden stress. The amplitude of wavy stylolites was as large as 1 cm (Fig. 11H). These types of stylolites were irregularly distributed throughout the strata at a depth ranging from 1000 to 4000 m. Based on the cross-cutting relationship in cores, at least two episodic stylolites exist that may have been influenced by variations in tectonic stress. Early-stage stylolites generally had horizontal or low dips, approximately parallel with bedding or lithologic interfaces, while late-stage stylolites were perpendicular to them (Fig. 10B, D). Also, pervasive brown or black bitumen stains were evident along these stylolites (Figs. 6I and 11K, L), indicating that they may have provided an excellent pathway for underground fluids, which widened and rounded the stylolites through dissolution (Fig. 11H).

4.3.2. Tiny pores and vugs associated with stylolites

Macroscopically, large numbers of tiny dotted dissolution pores and vugs were ubiquitous with different irregular shapes. They were observed with the naked eye as the maximum pore size noted in cores was up to 1.8 mm, and they were dispersedly distributed along or nearby stylolites and solution seams (Figs. 10A, C and 12A, F). Some vugs with residual calcite cement were visibly stained by crude oil (Fig. 12B). Moreover, in re-deposited brecciated micrite, dotted pores and vugs occurred in breccia particles rather than in the argillaceous fillings (Fig. 12H). Furthermore, there was no difference in the development of reticulate pores with nearly circular shapes, which are impenetrable and less connective (Fig. 12E). Microscopically, laminar dissolution pores arranged by independent pores were generally observed in thin sections (Fig. 11G). The fact that some of these pores were filled with bitumen or residual calcite cement demonstrates that pre-existing pores or vugs with calcite fillings create new space as they corrode (Figs. 11E, G and 12C, D). These features indicate that these pores and vugs formed in the mesogenetic environment with different degrees of erosion in different regions.

4.3.3. Dissolution enlarged fractures

As mentioned above, the Indosinian-Yanshanian tectonic event caused the development of high-angle fractures. Blocky calcites subsequently filled them in the mesogenetic environment (Fig. 5). However, these fractures were dissolved by corrosive fluids resulting in a sinuate edge, allowing them to be easily stained by hydrocarbons (Fig. 12G). Some fissures were formed by enlarged dissolution along pre-existing stylolites, which also brings about an expansion of adjacent fractures (Fig. 11H, I, M). In cores, such dissolution spaces along fractures were

commonly charged with brown crude oil or black bitumen (Fig. 12B).

4.3.4. Dissolution of late cement and hydrocarbon inclusions

The unsmoothed corrosion rim of late calcite cement in vugs that was observed in cores is indicative of dissolution that postdates precipitation, resulting in the formation of effective reservoir space (Fig. 12C and D), which was then re-filled with brown crude oil (Fig. 12B). Blocky calcites that precipitated in fractures (up to 1.2 mm in width) were cut by a stylolite, where the stylolite acted as a pathway for fluids, thus resulting in calcite dissolution (Fig. 11F). In addition, dissolution also occurred in blocky calcite cement that filled intergranular space in brecciated dolostone (Fig. 11C), and fractures in limestone and grainstone (Fig. 11J), and the erosion of poikilotopic calcite cement in giant spaces also formed a series of embayed or irregularly shaped vugs and pores (Fig. 11D, E). In particular, pre-existing vugs filled with saddle dolomite from the burial environment generated new effective vugs with irregular shapes by dissolution (Fig. 11B) and soluble seam-pores with black bitumen inclusions (Fig. 11A). By contrast, there was no distinct storage space in late calcite cemented in fractures and vugs, and these were sporadically eroded by pyrites (Figs. 10E, F and 11N) or siliceous fluids (Fig. 6L).

4.4. Geochemical features

Analytical results for trace elements and their normalizations to UCC (Rudnick and Gao, 2003), REEs and their normalizations to PAAS (McLennan, 1989), and isotopic compositions of the Ordovician carbonate rocks in the study area are listed in Table S2, Table S3, and Table S4, respectively.

4.4.1. Trace elements

The UCC-normalized trace element ratios for different types of samples are compared in the spider diagram presented in Fig. 13. In general, the UCC-normalized patterns of all samples were consistent (Fig. 13). However, the contents of most trace elements were relatively higher in eroded samples compared to uneroded samples of both dolostones (Fig. 13A) and limestones (Fig. 13B). For example, the Li, Sc, V, Cr, Co, Cu, and Zn contents in the eroded samples were typically higher than those in the uneroded samples, while the Sr, Sb, Ta, Ni, and U concentrations were very similar (refer to Table S2).

4.4.2. Rare earth elements (REEs)

As shown in Table S3 and Fig. 14, the total REE concentration (Σ REE) in every sample was lower than 100 ppm, indicating no contamination from terrestrial sources (Qing and Mountjoy, 1994). The Σ REE of eroded limestone samples varied from 9.475 ppm to 39.274 ppm with an average value of 23.157 ppm, which is higher than the average value of uneroded limestone samples (ranged from 5.629 ppm to 9.670 ppm with an average value of 7.361 ppm) (Table S3). Similar observations were made for dolostone samples. The Σ REE of eroded dolostone samples ranged from 3.689 ppm to 94.025 ppm with an average value of 29.150 ppm, while the Σ REE of uneroded dolostone samples ranged from 2.691 ppm to 16.085 ppm with an average value of 9.615 ppm (Table S3). After PAAS normalization, the REE partition patterns of eroded samples were consistent with those of uneroded samples. However, dolostone and limestone exhibited different features (Fig. 14). The dolostone samples were divided into two types, with most of them displaying right-leaning REE partition patterns characterized by light REE (LREE) enrichment and heavy REE (HREE) depletion (Fig. 14A). These were similar to all limestone samples (Fig. 14C), which indicates seawater-like dolomitized fluid modification. By contrast, the remaining dolomite samples exhibited left-leaning REE partition patterns with LREE depletion and HREE enrichment (Fig. 14B), which may indicate an influence by other diagenetic fluids.

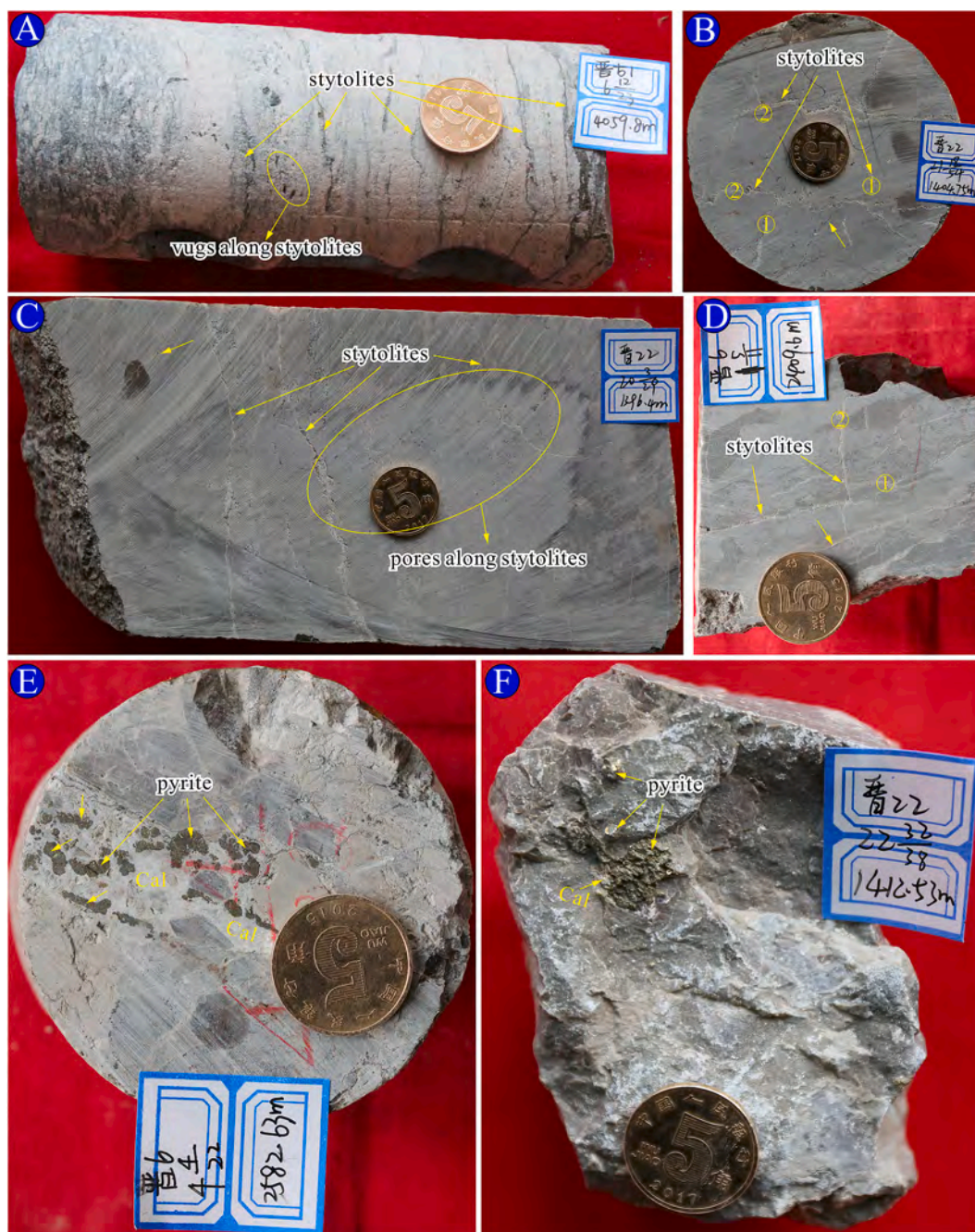


Fig. 10. Core photographs illustrating stylolites and related storage spaces, and pyrites metasomatism in previous calcites. (A) Grey micrite with stylolites, and vugs distributed along stylolites, well JG1, 4059.80m, O₂f. (B) Grey micrite with two generations of stylolite, well J22, 1404.75m, O₂m2. (C) Grey micrite with solution seams, and pores distributed along solution seams, well J22, 1396.40m, O₂m2. (D) Grey micrite with two generations of stylolite, well J6, 2409.60m, O₂m4. (E) Gray brecciated micrite with granular pyrites replacing the calcites precipitated in storage space, well J6, 2582.63 m, O₂m2. (F) Gray micrite with massive pyrites completely replacing the calcite in vugs, well J22, 1412.53m, O₂m2.

4.4.3. Oxygen and carbon isotopes

The cross-plotting analysis of $\delta^{13}\text{C}$ and $\delta^{18}\text{O}$ values and box-plotting analysis of $\delta^{13}\text{C}$ values from different samples are shown in Fig. 15A and C, respectively. The $\delta^{18}\text{O}$ values of all samples showed negative shifts of different degrees, and the $\delta^{18}\text{O}$ vs. $\delta^{13}\text{C}$ values in the cross-plot showed no correlation (Table S4; Fig. 15A).

The eroded limestone samples had $\delta^{13}\text{C}$ values ranging from -8.43‰ to -0.13‰ (average value -1.93‰), while the $\delta^{18}\text{O}$ values ranged from -10.52‰ to -8.26‰ with an average of -9.14‰ (Table S4). The uneroded limestone samples displayed $\delta^{13}\text{C}$ values ranging from -6.50‰ to -0.91‰ with a lower average value compared to that of

eroded samples (average value -3.12‰) (Table S4; Fig. 15A, C), while the $\delta^{18}\text{O}$ values ranged between -12.63‰ and -7.34‰ with an average value of -9.31‰ (Table S4).

The $\delta^{13}\text{C}$ values of eroded dolostone samples varied from -5.32‰ to $+0.25\text{‰}$ with a higher average value (-1.53‰) than that of uneroded samples (average value -1.93‰), which had $\delta^{13}\text{C}$ values ranging from -7.67‰ to $+0.38\text{‰}$ (Table S4; Fig. 15A, C). The $\delta^{18}\text{O}$ values of eroded dolostone samples ranged from -10.75‰ to -5.24‰ (average value -7.53‰), while uneroded samples had $\delta^{18}\text{O}$ values ranging from -9.41‰ to -5.98‰ (average value -7.24‰) (Table S4; Fig. 15A).

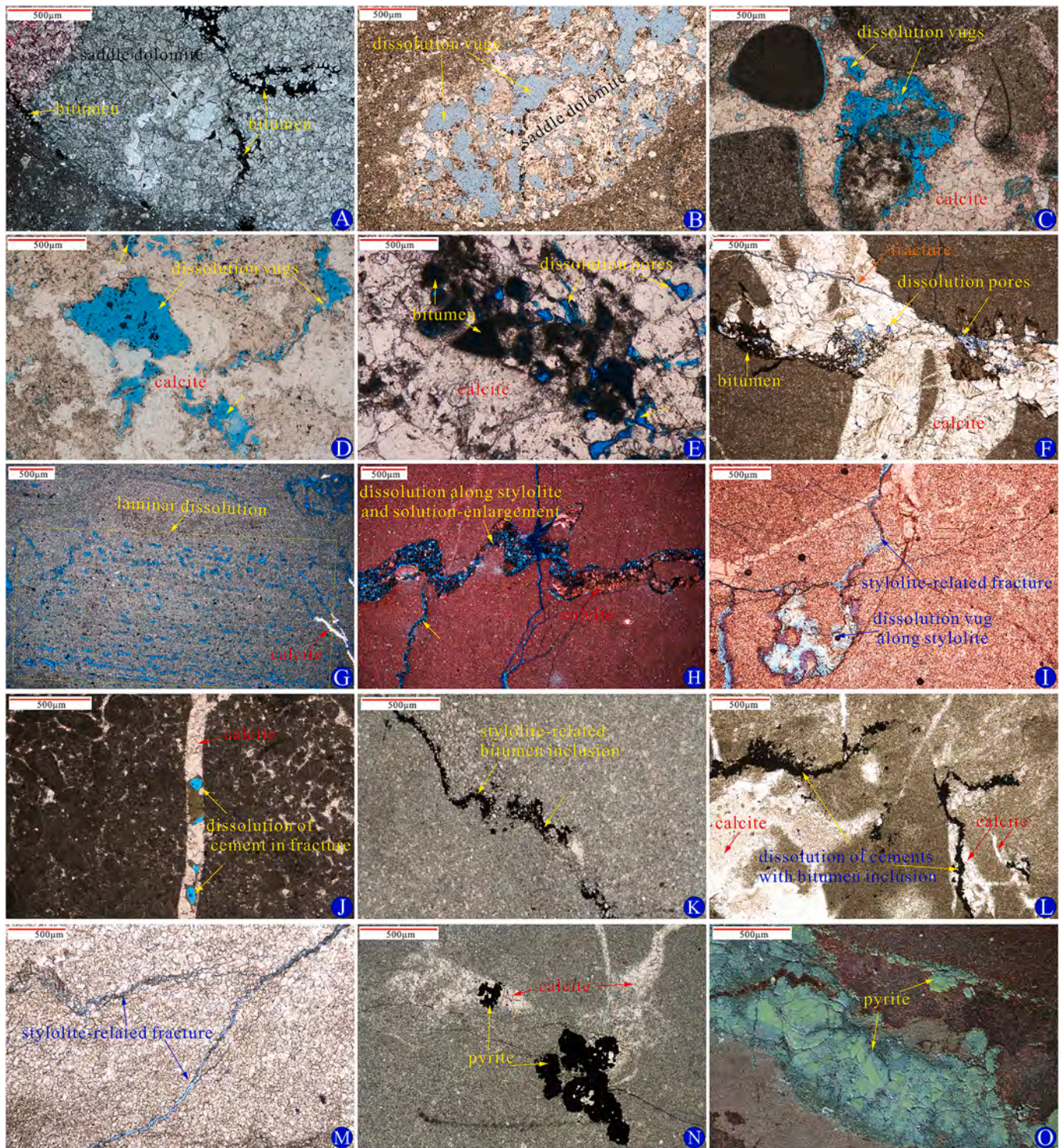


Fig. 11. Microphotographs displaying different phenomena of the mesogenetic dissolution (PPL-plane-polarized light; XPL-cross-polarized light; RL-reflected light). (A) Micrite with a vug filled with saddle and silty dolomites with bitumen stain, well J6, 2565.54 m, O₂m2, PPL. (B) Dolomiticrite with the dissolution of vug-filling saddle dolomite, well JG18, 1345.00 m, O₂m1, PPL. (C) Brecciated dolostone, the blocky calcites filled between breccias were eroded, well JG39, 1914.00 m, O₂m3, PPL. (D) Marlstone with dissolution vugs with irregular shapes, well JG23x, 1621.50 m, O₂f, PPL. (E) Dissolution in blocky calcites, well JG22x, 1637.15 m, O₂f, PPL. (F) Micrite, the dissolution of blocky calcite filled in fracture, well JG13, 4987.65 m, O₂f, PPL. (G) Dolomiticrite with laminar dissolution pores, well JG15, 1581.60 m, O₂m4, PPL. (H) Micrite, dissolution along stylolite and solution-enlargement, well JG22, 1405.06 m, O₂f, PPL. (I) Micrite with stylolite related-fracture and dissolution vug along stylolite, well JG1, 4058.20 m, O₂f, PPL. (J) Calcarenite, dissolution of calcite in fracture, well JG23x, 1621.00 m, O₂f, PPL. (K) Dolomitic micrite with stylolite-related bitumen inclusion, well J6, 2660.10 m, O₂m2, PPL. (L) Dolomitic micrite with bitumen stain in the dissolution of cement, well JG6, 3540.10 m, O₂f, PPL. (M) Silty crystalline dolostone with stylolite-related fracture, well JG14, 2221.70 m, O₂m2, PPL. (N) Micrite, pyrites replaced calcite in storage space, well J6, 2620.14 m, O₂m2, PPL. (O) Dolomiticrite, granular pyrites distributed along the fracture, well J6, 2640.00 m, O₂m2, RL.

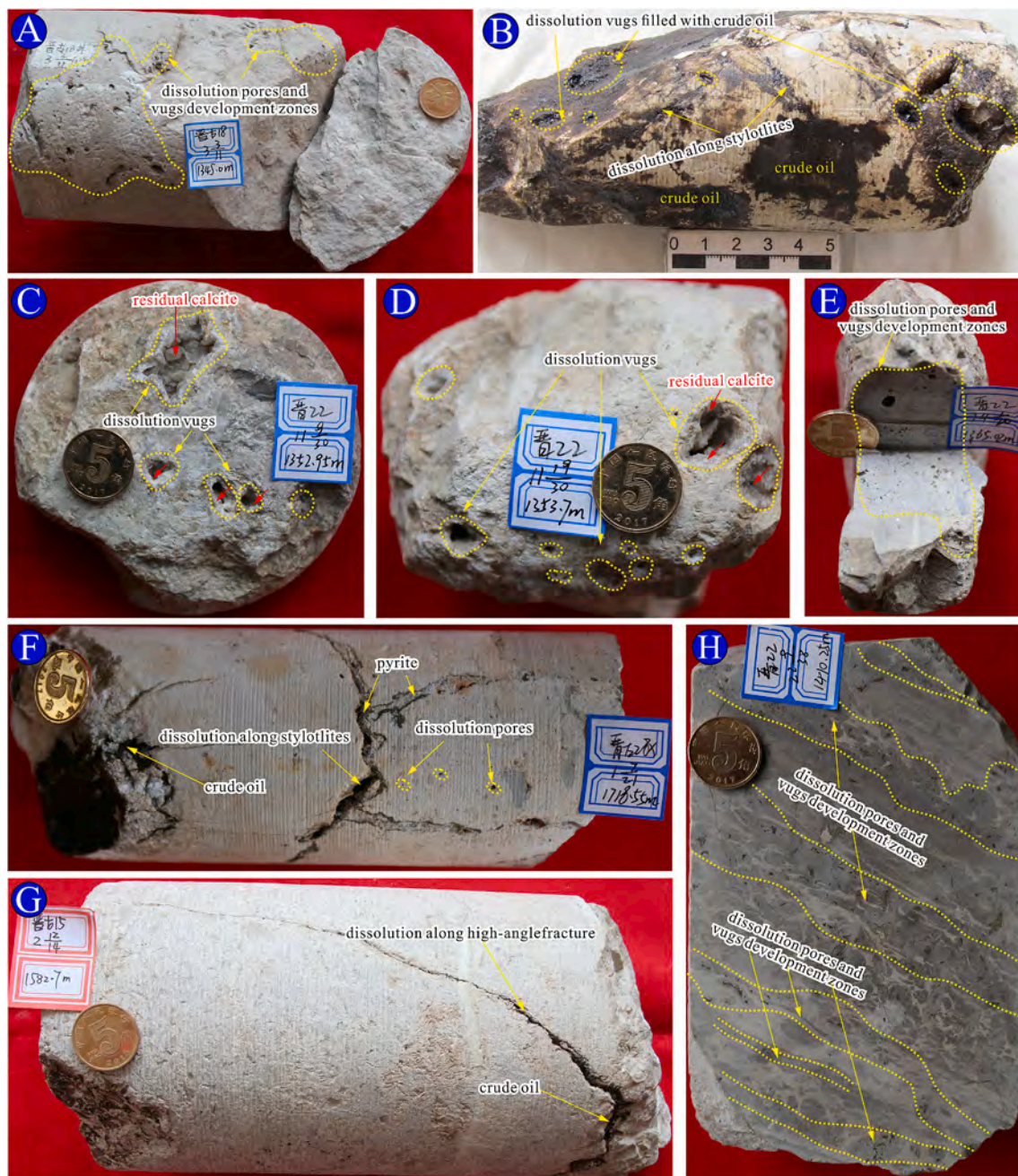


Fig. 12. Core photographs displaying different mesogenetic dissolution. (A) Greyish dolomitic micrite with numerous dissolution pores and vugs, well JG18, 1345.00 m, O₂m1. (B) Greyish-white dolomitic micrite, dissolution vugs filled with crude oil, well JG22x, 1637.82 m, O₂f. (C) Grey micrite, dissolution occurred in vug-filling calcites with different sizes, well J22, 1352.95 m, O₂m3. (D) Grey micrite, dissolution occurred in vug-filling calcites with different sizes, well J22, 1353.70 m, O₂m3. (E) Greyish dolomitic micrite with wide development of tiny pores and vugs, well J22, 1365.02 m, O₂m3. (F) Grey dolomitic micrite with development of pores and dissolution along stylolites, then were filled by crude oil and pyrites, well JG28x, 1718.22 m, O₂m2. (G) Greyish-white dolomitic micrite with dissolution along the high-angle fracture charged with crude oil, well JG15, 1582.70 m, O₂m4. (H) Grey brecciated micrite with multiple parallel dissolution pores and vugs development zones, well J22, 1410.25 m, O₂m2.

4.4.4. Strontium isotopes

The box-plotting analysis of $^{87}\text{Sr}/^{86}\text{Sr}$ ratios for Ordovician samples is shown in Fig. 16. Previous studies have reported an approximate range in values similar to that of Ordovician seawater (i.e., 0.707850–0.709100, Burke et al., 1982; Veizer et al., 1999). The $^{87}\text{Sr}/^{86}\text{Sr}$ ratios of all micrites nearly fell within this range, whereas dolostone samples had higher $^{87}\text{Sr}/^{86}\text{Sr}$ ratios (Fig. 16; Table S4). The $^{87}\text{Sr}/^{86}\text{Sr}$ ratios of eroded limestone samples ranged from 0.708667 to 0.709468 with an average value of 0.709060, and the two uneroded limestone samples that were measured had values of 0.709263 and

0.708933 (Table S4). Given the limited number of uneroded samples, $^{87}\text{Sr}/^{86}\text{Sr}$ ratios were not compared between eroded and uneroded limestone samples (Fig. 16). The $^{87}\text{Sr}/^{86}\text{Sr}$ ratios of eroded and uneroded dolostone samples ranged from 0.708925 to 0.711158 and from 0.709036 to 0.709395, respectively (Table S4). The average $^{87}\text{Sr}/^{86}\text{Sr}$ ratio of eroded samples (0.710164) was higher than that of uneroded samples (0.709261) (Table S4; Fig. 16).

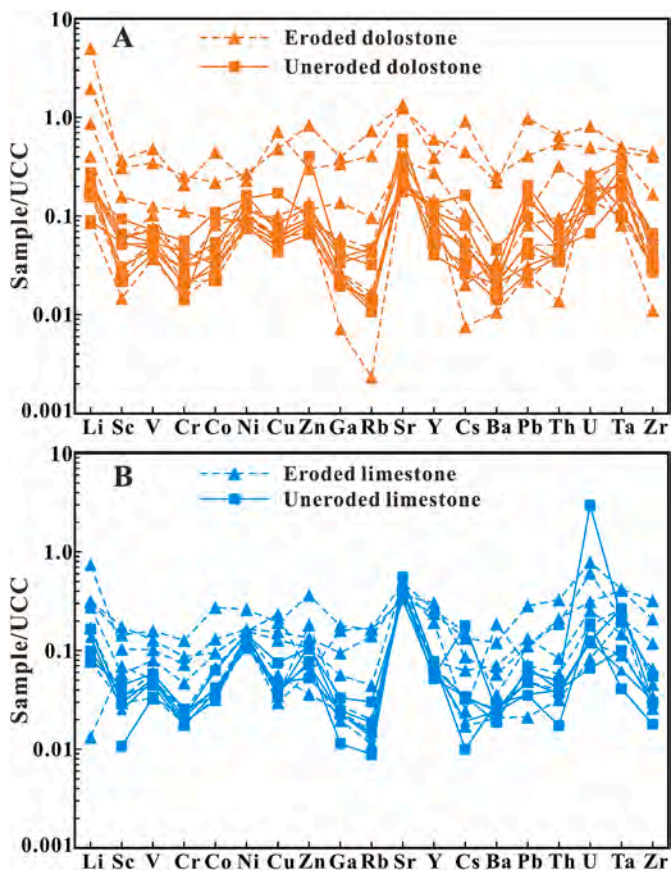


Fig. 13. Spider diagram of UCC-normalized trace elements in (A) dolostones and (B) limestones in the study area (UCC, Rudnick and Gao, 2003).

5. Discussion

5.1. Fluid types causing mesogenetic dissolution

Carbonate rocks are naturally dissolved by acidic solution because CO_3^{2-} ions in minerals tend to quickly bond with H^+ ions in calcite unsaturated water. However, connate fluids encapsulated in sediments at the syndepositional stage are unlikely to generate mesogenetic dissolution owing to their calcite saturated state caused by chemical equilibrium at an early stage of burial diagenesis (Jin et al., 2009). Many factors, including temperature, pressure, pH, fluid/rock ratio, mineral surface structure, and reaction surface area, control the interaction between rocks and fluids (Brantley and Conrad, 2008). The burial depth determines the temperature and pressure of a diagenetic system. Therefore, the relatively high temperature and pressure of the mesogenetic realm will effectively boost the rate of dissolution as demonstrated by many experimental simulations of carbonate dissolution (She et al., 2016; Ding et al., 2020). Meanwhile, there are usually two types of dissolution fluids: self-sourced fluids and external-sourced fluids, classified according to their origin (Moore and Druckman, 1981; Surdam et al., 1989; Zhu et al., 2007; Liu et al., 2008). As the name implies, self-sourced fluids are generally sourced from the rock itself (e.g., dehydration of gypsum and other evaporites, and clay mineral transformations). By contrast, external-sourced fluids are generated by other external geochemical and/or physical reactions, such as meteoric water, acidic materials (i.e., organic acids, CO_2 and H_2S), and hydrothermal fluids, which play a critical role in dissolution. Some studies have demonstrated that mesogenetic dissolution is a composite result caused by self- and/or external-sourced corrosive fluids (Zhu et al., 2007; Liu et al., 2008).

Meteoric water, as the primary aggressive fluid in the subaerial environment, easily erodes carbonates to form secondary porosity (Longman, 1980; James and Choquette, 1984; Mazzullo and Harris, 1991; Mazzullo, 2004; Moore and Wade, 2013). Meanwhile, it may also bring mesogenetic pores into existence, generated by deep meteoric

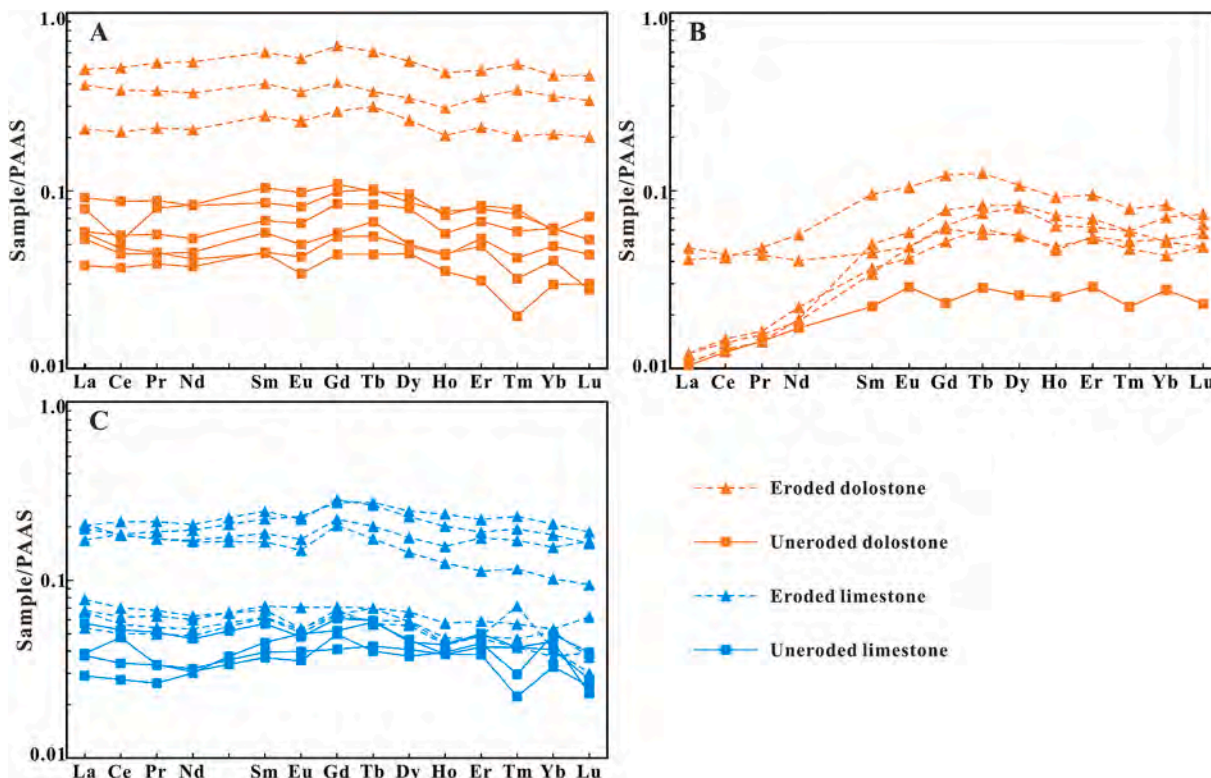


Fig. 14. PAAS-normalized rare earth elements partition pattern of dolostones (A and B) and limestones (C) (PAAS, McLennan, 1989).

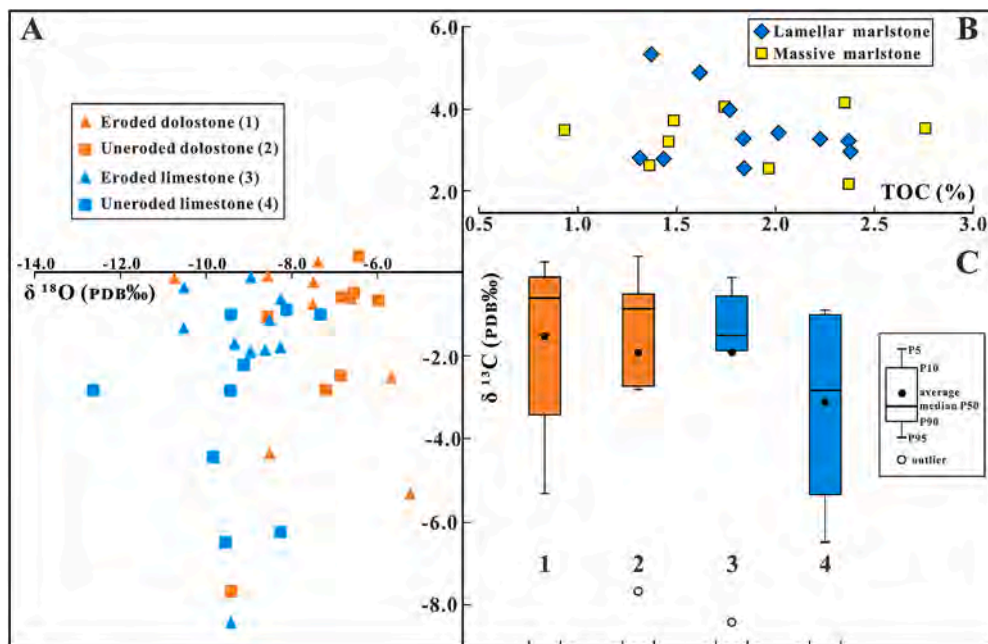


Fig. 15. (A) Cross-plot showing carbon-oxygen isotopic compositions in eroded and uneroded samples. (B) Cross-plot displaying the relationship between TOC content (%) and carbon isotopic compositions of lamellar and massive marlstone in Es_3^1 (from Li, 2015). (C) Box-plot of carbon isotopic compositions of different samples (see Fig. 15A).

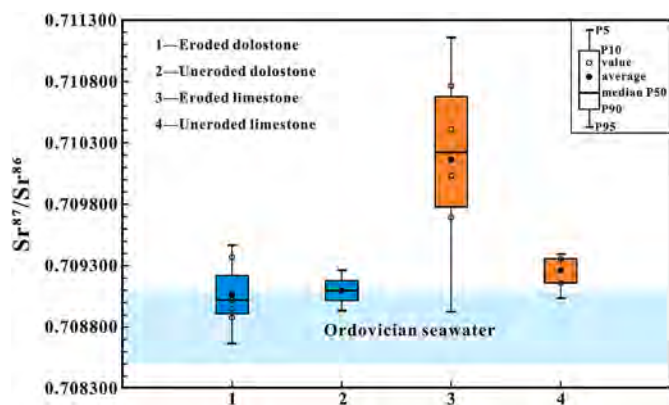


Fig. 16. The boxplot showing the $\text{Sr}^{87}/\text{Sr}^{86}$ ratios of different carbonates in the study area.

water recharge in many tilted or faulted basin strata (Toth, 1980) or modified meteoric water derived from the crystalline basement (Aschwanden et al., 2019). In general, there is a lot of evidence showing that a large number of acidic materials generated from organic maturation or thermal degradation during the burial stage, such as organic acids, CO_2 , and H_2S , can easily influence subsurface rocks (Moore and Druckman, 1981; Crossey et al., 1986; Surdam et al., 1989; Mazzullo and Harris, 1991; Seewald, 2003; Lambert et al., 2006; Zhu et al., 2007; Jin et al., 2009; Feng et al., 2013; Ding et al., 2020). However, Biehl et al. (2016) considered that CO_2 alone has a negligible effect on carbonate dissolution in a closed system unless combined with a low pH environment caused by dolomitization or pyrite formation by TSR-derived H_2S (Hao et al., 2015). Therefore, organic acids, acidic CO_2 -charged water under specific conditions or undersaturated fluid associated with kerogen (hydrocarbon-bearing) in subsurface resource rocks, have been regarded as the most likely fluids to cause mesogenetic dissolution in carbonates (Mazzullo and Harris, 1992; Seewald, 2003; Zhu et al., 2007; Liu et al., 2008; Jin et al., 2009; Feng et al., 2013; Ding et al., 2020). Many simulation experiments of carbonate reservoir modification have also

indicated that acidic fluids associated with resource rock can erode carbonate rocks, thus improving porosity. However, the process is controlled by the calcium carbonate saturation, fluid velocity, water/rock ratio, and primary pore structure (Ding et al., 2020). In addition, CO_2 or other inorganic acidic fluids released from magmatism or basement rocks also influence rocks in the mesogenetic zone, a fact that has been supported by Jiang et al. (2015) and Valencia and Laya (2020). Moreover, it is well known that thermochemical sulfate reduction (TSR) can lead to deep carbonate dissolution (e.g., Hao et al., 2015; Jia et al., 2016), and that hydrothermal fluids migrating along faults can dissolve carbonate strata and precipitate saddle dolomite (e.g., Davies and Smith, 2006; Bai et al., 2020). Finally, there are other fluid types that also play an essential role in mesogenetic dissolution, such as fluids derived from reverse weathering reactions (Lundegard and Land, 1986), fluids evolved through the dehydration of gypsum and other evaporites (Moore and Druckman, 1981; Kendall, 1984; Machel and Anderson, 1989; Surdam et al., 1989) or fluids generated during clay mineral transformations, i.e., the conversion of smectite to illite (Foscolos, 1984), and released during mudstone/shale compaction (Hower et al., 1976; Xu et al., 2017). As mentioned above, fluids causing mesogenetic dissolution generally migrate along faults, bedding planes, formational boundaries, fractures, and even non-permeable beds (Mazzullo and Harris, 1992; Feng et al., 2013).

5.2. Identification of likely fluids in the current study

By combining petrography with geochemical analysis, it was possible to identify the likely fluids involved in mesogenetic dissolution (Zhu et al., 2007; Liu et al., 2008; Jin et al., 2009). First, the petrography results revealed that the phenomena of mesogenetic dissolution are ubiquitous in the current study area, which primarily displayed characteristics of external-sourced dissolution, such as large, visible, and interconnected dissolved pores and vugs, and corrosion along stylolites and fractures (Figs. 10–12). Meanwhile, brown to black bitumen that was widely distributed along or in stylolites and fractures or related dissolution pores (Figs. 11A, E, K, L, N and 12B, F, G) was well preserved, and pyrites occurred in pores distributed along fractures (Figs. 10E, F and 11O). These phenomena suggest that dissolution may

have been associated with hydrocarbon-bearing fluids (Feng et al., 2013). Second, fluid-rock reactions can alter the isotope and trace element chemistry of rocks (Nabelek, 1987). Thus, fluids resulting in mesogenetic dissolution should overprint some common characteristics with resource fluids, including trace elements and REEs (Jin et al., 2009). Organic matter is enriched in trace elements relative to the whole rock (Tait, 1987), and some trace elements like Co, Cr, Cu, Mo, Ni, V, and Zn are usually abundant in organic matter-rich sediments (e.g., Vine and Tourtelot, 1970; Brumsack, 1980). Their enrichment in the sediment can be ascribed to (1) progressive accumulation in organic tissues, (2) precipitation with sulphides in anoxic environments assisted by preserved organic matter, or (3) post-depositional diagenetic alteration (Brumsack, 1980; Nijenhuis et al., 1999). Excepting the above-mentioned Co, Cr, Cu, Ni, V, and Zn, other trace elements in eroded limestone and dolostone samples also had relatively higher concentrations compared to uneroded samples (Table S2; Fig. 13). Meanwhile, the UCC-normalized patterns of these trace elements were consistent with those of uneroded samples (Fig. 13). Therefore, dissolved fluids that increase trace element concentrations in eroded rocks through element substitution or intrusion can similarly be inferred to be hydrocarbon-bearing fluids derived from organic matter-rich source rock. In addition, the eroded and uneroded samples showed similar PAAS-normalized REE patterns, which may reflect a previous influence of diagenetic fluid (Fig. 14). Most importantly, the measured REE concentrations in all eroded samples were 5–10 times greater than those in uneroded samples (Fig. 14; Table S3). Organic matter not only is able to accumulate REEs but also leads to a pronounced REE fractionation during diagenetic degradation (Felitsyn and Morad, 2002). Therefore, the acidic materials generated from organic diagenesis in source rock can alter the pH condition of the fluid-rock reaction system to subsequently release REEs into hydrocarbon-bearing fluids (Nesbitt, 1979; Duddy, 1980; Möller and Bau, 1993). Thus, it can be concluded that hydrocarbon-bearing fluid that migrated into Ordovician strata in the study area caused the REE enrichment in eroded parts through fluid-rock interaction (e.g., mesogenetic dissolution). Finally, the mesogenetic zone is located at a certain burial depth (Choquette and Pray, 1970) where the temperature of the fluid is relatively high. The $\delta^{18}\text{O}$ values of all samples showed pronounced negative shifts (Fig. 15A), which for carbonate compositions is attributed to the fact that the diagenetic fluid-rock interaction took place at high temperature and pressure (Taylor, 1974; Anderson and Arthur, 1983). The $\delta^{13}\text{C}$ values were relatively stable compared to the $\delta^{18}\text{O}$ values, mainly depending on the organic carbon content and hydrocarbon (CH_4) origin or conversion in rock (Chen, 1994). Although most of the values displayed slightly negative shifts (Table S4; Fig. 15A), the average $\delta^{13}\text{C}$ values of eroded dolostone and limestone were greater than the average values of corresponding uneroded samples (Table S4; Fig. 15C). The $\delta^{13}\text{C}$ values of lamellar and massive marlstone with different TOC content in the lower part of the Sha3 member (Es_3^1) showed positive shifts (Li, 2015, Fig. 15B). Presumably, eroded samples might have slightly higher carbon isotope compositions as these were altered by the hydrocarbon-bearing fluid derived from marlstone. Moreover, the hydrocarbon-bearing fluid from lacustrine marlstone should have higher $^{87}\text{Sr}/^{86}\text{Sr}$ ratios due to a continental crust in origin (Liang et al., 2007; Elderfield, 1986). Therefore, compared with the eroded samples, especially dolostone, the uneroded samples had higher $^{87}\text{Sr}/^{86}\text{Sr}$ ratios (Fig. 16; Table S4).

In summary, based on the above analysis, we suggest that the most likely fluids causing mesogenetic dissolution in the study area are mainly acidic fluids associated with organic matter maturation in resource rocks, i.e., a composite mixture of organic acids, CO_2 , or a little H_2S as corrosive fluids, from the overlying clastic rock strata (i.e., organic matter-rich marlstone in the lower part of the Sha3 member).

5.3. Formation mechanism of mesogenetic dissolution and the influence of mesogenetic dissolution on the reservoir

5.3.1. Mesogenetic dissolution model

The most critical conditions that must be met for mesogenetic changes to occur in carbonate rocks can be narrowed to the following three: (1) having sufficient volumes of fluids migrating through effective conduits; (2) having fluids that can react with rocks either in dissolution or cementation processes; and (3) having fluids that remain undersaturated with respect to calcium carbonate (Mazzullo and Hariss, 1992). In the study area, marlstones intercalated with E_3s^1 mudstones are very pervasive, and organic matter-rich marlstone ($\text{TOC} > 1\%$) with a thickness greater than 100 m covers a large area (more than 300 km^2) of the Shulu Sag (Huo et al., 2019). A large quantity of hydrocarbons and corresponding fluids were produced as the organic matter in marlstones matured, and these hydrocarbons were expelled radially from source rock kitchens in the sub-sag zone, and then migrated westward to the gentle slope (Ren et al., 2019). Cai et al. (2020) suggested that the timing of organic matter maturation in the E_3s^1 is from the early period of Ed (ca. 30 Ma) to the present-day. The surface of the unconformity between the Ordovician and Eocene-Pliocene terrestrial strata played a crucial role in hydrocarbon migration (Zou et al., 2015; Cai et al., 2020). In addition, other discontinuity surfaces in Ordovician rocks, such as pores, cracks, faults, fractures, bedding planes, and stylolites, are also excellent conduits for these chemically aggressive fluids, because they act as “localized points of influx” (Wright and Harris, 2013). The conditions described above are conducive to mesogenetic dissolution.

Fig. 17 illustrates the causal mechanism of mesogenetic dissolution affecting Ordovician rocks in the study area. A stage of large-scale oil and gas generation occurred during the early period of Ed deposition; however, it was difficult for hydrocarbons to migrate into the hydrocarbon supply window because there was not enough driving pressure (Cai et al., 2020). Meteoric water in the subaerial exposure zone might migrate into relatively deep strata due to the gravitational potential energy of fluids in the updip-tilted Ordovician strata (Fig. 17A). However, the mineral-fluid reaction in carbonate rocks quickly achieved chemical equilibrium as fluids infiltrated downward from the surface (Banner and Hanson, 1990). Therefore, there was little chance of generating ubiquitous mesogenetic dissolution. However, from the Neogene-Quaternary period to the present, organic matter in the marlstone of E_3s^1 continued to mature, thus allowing for hydrocarbon-bearing fluids to easily reach the hydrocarbon supply window and migrate into Ordovician strata (Cai et al., 2020). Ordovician sedimentation also occurred in the mesogenetic environment (Figs. 4h, 5 and 17B). In addition, both the Cambria Formation and Carboniferous-Permian consist of multi-phased mudstone and/or coal layers, which are effective impermeable beds (An et al., 1982; Lao and Gao, 1984; Chen and Meng, 1993, Figs. 2 and 17) that act as fluid-resisting layers. The continuous underlying-sediments (Q-N Formation) may have caused released water to transport into the tilted Ordovician strata along unconformities and stylolites. At the same time, these fluids, altered by acidic materials contained in the hydrocarbon-bearing fluids from the hydrocarbon supply window, were undersaturated, and could easily generate dissolution space in deeper areas (Fig. 17B). The combination of the tilted structural shape of the basin and good conduits (i.e., unconformity, stylolites, and fractures) provides favorable conditions for aggressive fluids from organic-rich marlstones in the lower part of the Sha3 member (Es_3^1) to efficiently migrate laterally along conduits into the Ordovician strata where they cause erosion leading to mesogenetic dissolution. Simultaneously, the continual charging of oil and gas plays a protective role in porosity preservation. Therefore, many mesogenetic dissolution belts in the burial environment provide a series of considerable micro- and macroscopic storage space (Fig. 17B).

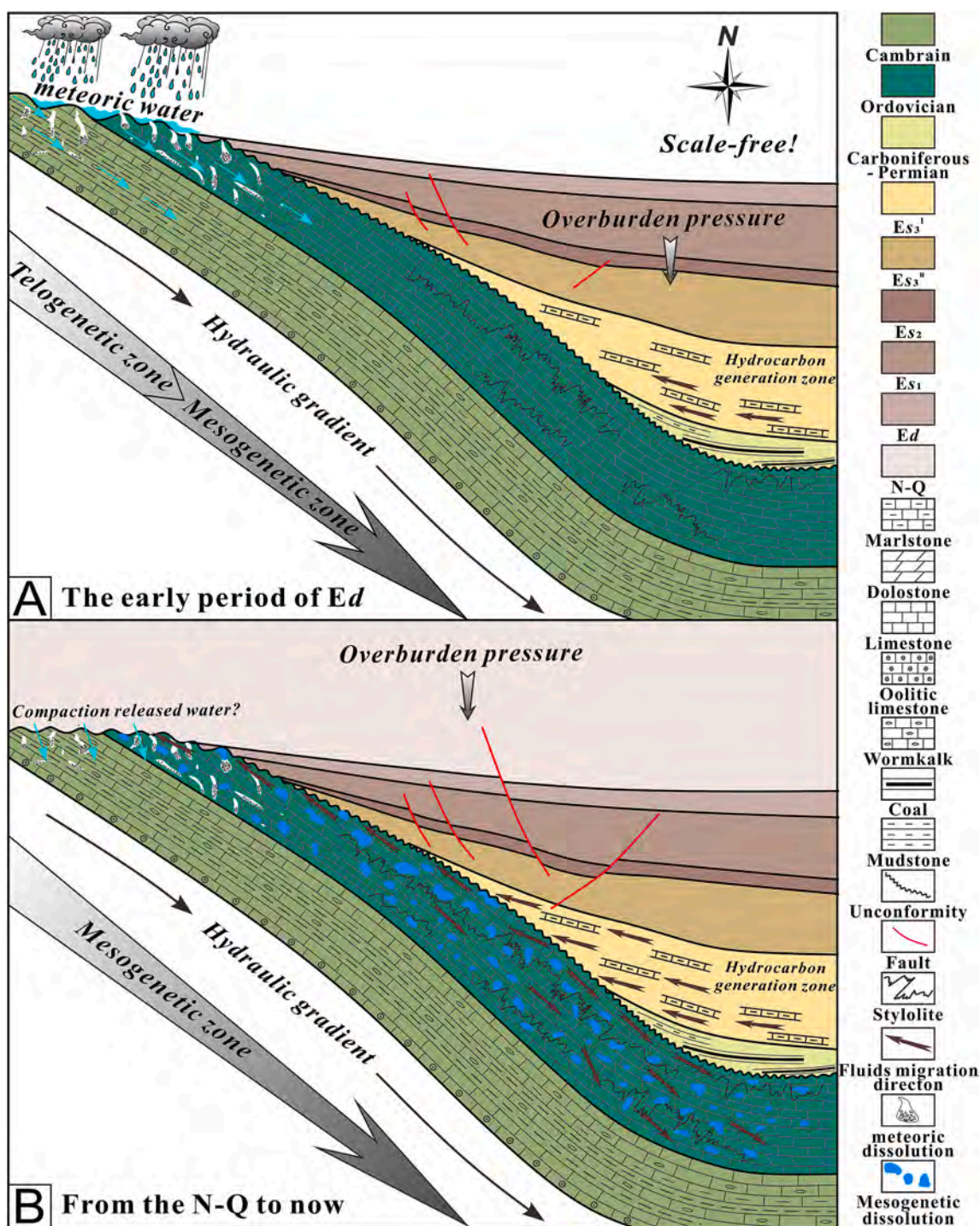


Fig. 17. Schematic diagram showing the mesogenetic dissolution processes of the Ordovician strata in the western slope of the Shulu Sag.

5.3.2. Influence on reservoir development

Based on wireline log porosity interpretation, it is apparent that good reservoirs (porosity > 5%) have developed in the western slope of the Shulu Sag (Fig. 18). Belts of good reservoir are distributed as discontinuous multilayers extending from the unconformity surface to deep burial carbonate rocks (Fig. 18). High-quality reservoirs in close proximity to the unconformity were likely formed predominantly by meteoric water leaching. However, well J8 and the lower parts of wells J22 and J6, which are far away from the unconformity with a relatively deeper burial depth, have also developed high-quality reservoirs, in which a large amount of water was produced during hydrocarbon

production (Fig. 18). Therefore, there is no doubt that mesogenetic dissolution can contribute in part to the total porosity in reservoirs and improve reservoir quality. However, there is no evidence of any detailed evaluation that has examined the degree of porosity increase related to mesogenetic dissolution. The reason for this may be attributed to the following: (1) the mesogenetic porosity is a complex process and the question of where it occurs in the subsurface cannot be answered with the present level of understanding (Mazzullo and Hariss, 1992); (2) the reservoir porosity of current samples consists of several different porosity types; and, (3) there is currently a lack of continuous dense sampling from any well in the study area. Nevertheless, the current

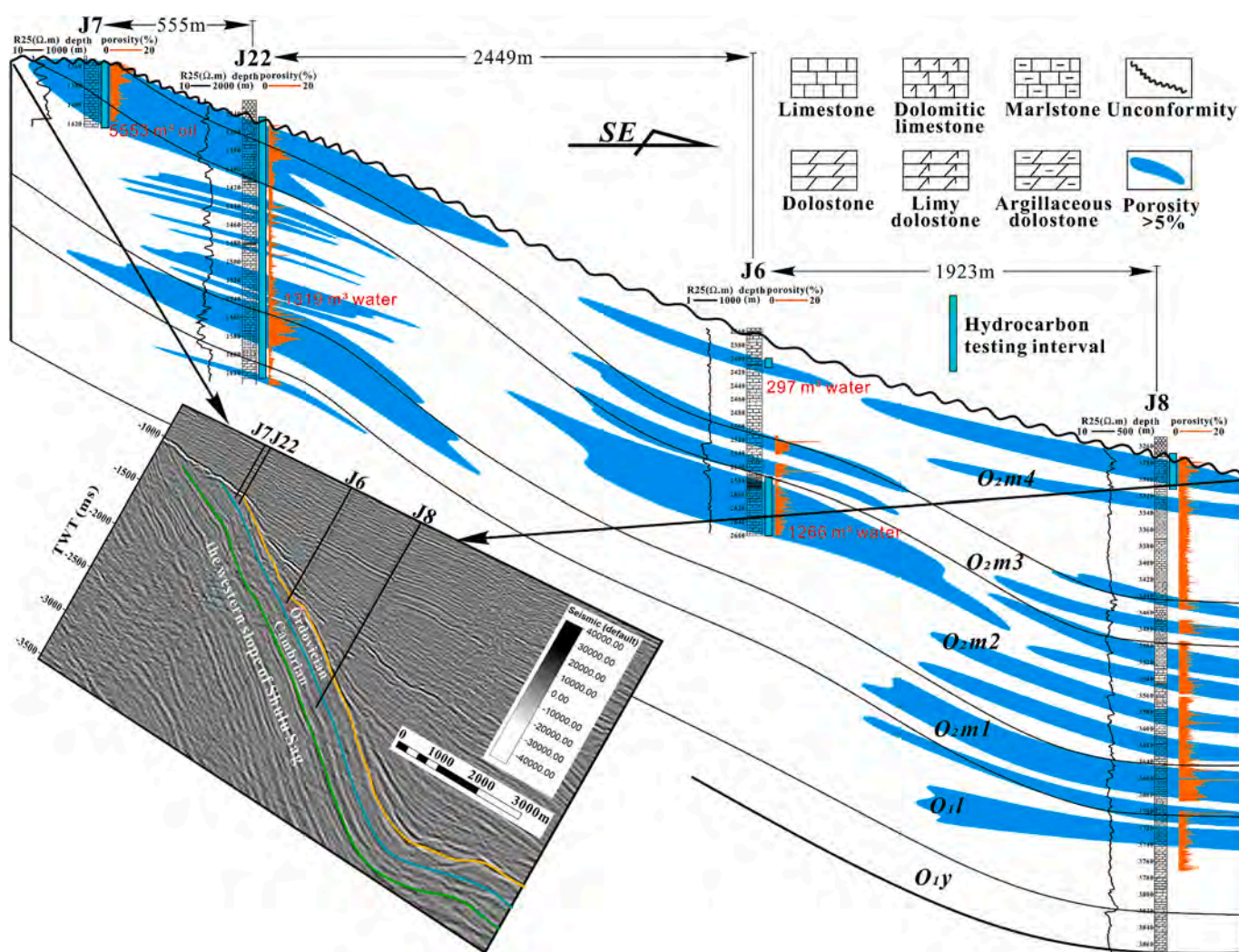


Fig. 18. The well-section profile showing the distribution of high-quality reservoir in the southwestern slope of the Shulu Sag based on wireline log porosity and hydrocarbon production testing intervals.

study of mesogenetic dissolution still provides new insight for future hydrocarbon exploration.

6. Conclusions

- (1) Based on the synthesis of stratigraphy and basin architecture, the tectonic evolution of the Shulu Sag can be defined as having a four-stage growth history. Combined with the burial history, the carbonate rocks in the study area have mainly been altered by three different diagenetic stages (i.e., syngenetic, telogenetic, and mesogenetic). The presence of abundant stylolites, tiny dotted dissolution pores and vugs associated with stylolites, dissolution enlarged fractures, erosion of late cement (e.g., saddle dolomite), and related hydrocarbon inclusions indicate that mesogenetic dissolution is ubiquitous in the Ordovician rocks in the study area.
- (2) UCC-normalized trace element and PAAS-normalized REE partition patterns of eroded samples are consistent with those of uneroded samples. Compared with uneroded samples, the eroded samples have higher contents of some trace elements (e.g., Co, Cr, Cu, Ni, V, and Zn) and REEs, and relatively higher average $\delta^{13}C$ values and $^{87}Sr/^{86}Sr$ ratios, indicating that the most likely corrosive fluids causing dissolution are acidic materials in hydrocarbon-bearing fluids, which may have been derived from

the maturation of organic matter in marlstone in the lower part of the Sha3 member (Es_3^1).

- (3) During the early period of Ed deposition, there was little chance to generate ubiquitous mesogenetic dissolution. Since the N-Q period however, the combination of the tilted structural shape of the basin and presence of good conduits (i.e., unconformity, stylolites, and fractures) has caused corrosive fluids from organic-rich marlstones in the Es_3^1 to laterally migrate into Ordovician strata more efficiently resulting in perfect mesogenetic dissolution that has led to the formation of a series of considerable micro- and macroscopic storage space. Mesogenetic dissolution can contribute in part to the total porosity in reservoirs and improve reservoir quality, a fact that provides new insight into future hydrocarbon exploration.

Author statement

Pengfei Xiang: Conceptualization, Writing – original draft, Resources; Hancheng Ji: Supervision, Funding acquisition; Yanqing Shi: Supervision, Writing – review & editing; Yebo Du: Writing – review & editing; Peng Chen: Writing – review & editing; Qingping Weng: Supervision, investigation; Xinrong Xu: Investigation; Yushu Sun: Investigation; Yun Huang: Validation, Resources; Shuqi Zou: Investigation.

Declaration of competing interest

The authors declare that they have no known competing financial interests or personal relationships that could have appeared to influence the work reported in this paper.

Acknowledgements

This work was supported by the National Key Research and Development Program of China (Grant Numbers 2018YFC0604301 and 2019YFB1504101), the CNPC Science & Technology Major Project (Grant Number 2017E-15), and the open projects of China University of Petroleum (Beijing) (PRP/indep-3-1817, PRP/open-1613). We appreciate Executive Editor Dr. Tahar Aïfa, Dr. Tina Drexler, and anonymous reviewers for their constructive comments and suggestions to improve the manuscript. We also thank Huabei Oilfield Branch Company (CNPC) for their supporting data and help.

Appendix A. Supplementary data

Supplementary data to this article can be found online at <https://doi.org/10.1016/j.petrol.2021.109045>.

References

- An, Taiyang, Wang, Xiping, An, Zuoxiang, 1982. Lithologic identification of Cambrian and Ordovician in North China and their oil potentials. *Oil Gas Geol.* 3 (2), 158–169.
- Anderson, T.F., Arthur, M.A., 1983. Stable isotopes of oxygen and carbon and their application to sedimentologic and paleoenvironmental problems. In: Arthur, M.A. (Ed.), *Stable Isotopes in Sedimentary Geology*, vol. 10. SEPM Short Course, pp. 1–151.
- Aschwanden, L., Diamond, L.W., Mazurek, M., Davis, D.W., 2019. Creation of Secondary Porosity in Dolostones by Upwelling Basement Water in the Foreland of the Alpine Orogen, vol. 2019. *Geofluids*, pp. 1–23.
- Bai, H., Huang, W., Wu, F., Ma, B., Wang, W., 2020. Mesogenetic diagenesis of the ordovician limestone in yubei area, Tarim Basin, NW China. *Carbonates Evaporites* 35 (3), 1–18.
- Banner, J.L., Hanson, G.N., 1990. Calculation of simultaneous isotopic and trace element variations during water-rock interaction with applications to carbonate diagenesis. *Geochem. Cosmochim. Acta* 54 (11), 3123–3137.
- Barnett, A.J., Wright, V.P., Chandra, V.S., Jain, V., 2015. In: *Distinguishing between Eogenetic, Unconformity-Related and Mesogenetic Dissolution: a Case Study from the Panna and Mukta Fields, Offshore Mumbai, India*, SP 435. Geological Society, London, Special Publications, pp. 67–84.
- Biehl, B.C., Reuning, L., Schoenherr, J., Lewin, A., Leupold, M., Kukla, P.A., 2016. Do CO₂-charged fluids contribute to secondary porosity creation in deeply buried carbonates? *Mar. Petrol. Geol.* 76, 176–186.
- Brantley, S.L., Conrad, C.F., 2008. Analysis of rates of geochemical reactions. In: *Kinetics of Water-Rock Interaction*. Springer, New York, NY, pp. 1–37.
- Brumsack, H.J., 1980. Geochemistry of cretaceous black shales from the atlantic pcean (DSDP legs 11, 14, 36 and 41). *Chem. Geol.* 31, 1–25.
- Burke, W.H., Denison, R.E., Hetherington, E.A., Koepnick, R.B., Nelson, H.F., Otto, J.B., 1982. Variation of seawater ⁸⁷Sr/⁸⁶Sr throughout Phanerozoic time. *Geology* 10 (10), 516–519.
- Burchette, T.P., 2012. Carbonate rocks and petroleum reservoirs: a geological perspective from the industry. Geological Society, London, Special Publications 370 (1), 17–37.
- Cai, Chuan, Qiu, Nansheng, Liu, Nian, Li, Zhenming, Wang, Yuanjie, Yu, Zhanwen, Jiao, Yaxian, 2020. Unconformity characteristics, hydrocarbon migration, and the accumulation model of the burial hill in the Shulu sag, Jizhong depression. *Acta Geol. Sin.* 94 (3), 888–904.
- Chen, Rongkun, 1994. Application of stable oxygen and carbon isotope in the research of carbonate diagenetic environment. *Acta Sedimentol. Sin.* 12 (4), 11–21.
- Chen, Rongkun, Meng, Xianghua, 1993. Early Palaeozoic sedimentary suites and the evolution of the north China platform. *J. Palaeogeogr.* 13 (4), 46–55.
- Choquette, P.W., Pray, L.C., 1970. Geologic nomenclature and classification of porosity in sedimentary carbonates. *AAPG Bull.* 54 (2), 207–250.
- Crossey, L.J., Surdam, R.C., Lahann, R.W., 1986. Application of organic/inorganic diagenesis to porosity pre diction. In: Gautier, D.L. (Ed.), *Roles of Organic Matter in Sediment Diagenesis: SEPM Special Publication*, vol. 38, pp. 147–156.
- Davies, G.R., Smith, L.B., 2006. Structurally controlled hydrothermal dolomite reservoir facies: an overview. *AAPG (Am. Assoc. Pet. Geol.) Bull.* 90, 1641–1690.
- Ding, Qian, He, Zhiliang, Wang, Jingbin, Zhu, Dongya, 2020. Simulation experiment of carbonate reservoir modification by source rock-derived acidic fluids. *Oil Gas Geol.* 41 (1), 223–234.
- Duddy, L.R., 1980. Redistribution and fractionation of rare-earth and other elements in a weathering profile. *Chem. Geol.* 30 (4), 363–381.
- Ehrenberg, S.N., Walderhaug, O., Bjørlykke, K., 2012. Carbonate porosity creation by mesogenetic dissolution: reality or illusion? *AAPG Bull.* 96 (2), 217–233.
- Elderfield, H., 1986. Strontium isotope stratigraphy. *Palaeogeogr. Palaeoclimatol. Palaeoecol.* 57 (1), 71–90.
- Fabricius, I.L., 2003. How burial diagenesis of chalk sediments controls sonic velocity and porosity. *AAPG Bull.* 87 (11), 1755–1778.
- Felitsyn, S., Morad, S., 2002. REE patterns in latest Neoproterozoic–early Cambrian phosphate concretions and associated organic matter. *Chem. Geol.* 187 (3–4), 257–265.
- Feng, Jinlai, Cao, Jian, Hu, Kai, Peng, Xiaoqun, Chen, Yan, Wang, Yanfei, Wang, Mu, 2013. Dissolution and its impacts on reservoir formation in moderately to deeply buried strata of mixed siliciclastic–carbonate sediments, northwestern Qaidam Basin, northwest China. *Mar. Petrol. Geol.* 39 (1), 124–137.
- Feng, Zengzhao, Chen, Jixin, Wu, Shenghe, 1989. Early paleozoic lithofacies and paleogeography of the north China platform. *Acta Sedimentol. Sin.* 7 (4), 15–55.
- Feng, Zengzhao, Jin, Zhenkui, 1994. Types and origin of dolostones in the lower palaeozoic of the north China platform. *Sediment. Geol.* 93 (3–4), 279–290.
- Foscolos, A.E., 1984. Diagenesis 7. Catagenesis of argillaceous sedimentary rocks. *Geosci. Can.* 11, 67–75.
- Friedman, G.M., 1959. Identification of carbonate minerals by staining methods. *J. Sediment. Res.* 29 (1), 87–97.
- Garrison, R.E., 1981. Diagenesis of oceanic carbonate sediments: a review of the DSDP perspective. In: Warme, J.E., Douglas, R.G., Winterer, E.L. (Eds.), *The Deep Sea Drilling Project: A Decade of Progress*, vol. 32. SEPM Sp. Publ., pp. 181–207.
- Goldhammer, R.K., 1997. Compaction and decompaction algorithms for sedimentary carbonates. *J. Sediment. Res.* 67 (1), 26–35.
- Halley, R.B., Schmoker, J.W., 1983. High-porosity Cenozoic carbonate rocks of south Florida: progressive loss of porosity with depth. *AAPG (Am. Assoc. Pet. Geol.) Bull.* 67 (2), 191–200.
- Hao, F., Zhang, X., Wang, C., Li, P., Guo, T., Zou, H., Zhu, Y., Liu, J., Cai, Z., 2015. The fate of CO₂ derived from thermochemical sulfate reduction (TSR) and effect of TSR on carbonate porosity and permeability, Sichuan Basin, China. *Earth Sci. Rev.* 141, 154–177.
- Hou, Guiting, Qian, Xianglin, Song, Xinmin, 1998. The origin of the Bohai Bay Basin. *Acta Sci. Nauralium Univ. Pekin.* 34 (4), 46–55.
- Hower, J., Eslinger, E.V., Hower, M.E., Perry, E.A., 1976. Mechanism of burial metamorphism of argillaceous sediment: 1. Mineralogical and chemical evidence. *Geol. Soc. Am. Bull.* 87 (5), 725–737.
- Hu, Yongjie, Cai, Chunfang, Pederson, Chelsea L., Liu, Dawei, Jiang, Lei, He, Xunyun, Shi, Shuyuan, Immenhauser, Adrian, 2020. Dolomitization history and porosity evolution of a giant, deeply buried Ediacaran gas field (Sichuan Basin, China). *Precambrian Res.* 338, 105595.
- Huo, Z., Tang, X., Meng, Q., Zhang, J., Li, C., Yu, X., Yang, X., 2019. Geochemical characteristics and hydrocarbon expulsion of lacustrine marlstones in the Shulu sag, Bohai Bay Basin, eastern China: assessment of tight oil resources. *Nat. Resour. Res.* 1–23.
- James, N.P., Choquette, P.W., 1984. Diagenesis 9. Limestones—the meteoric diagenetic environment. *Geosci. Can.* 11, 161–194.
- Jia, Zhenyuan, Hao, Shisheng, 1989. Formation and Distribution of Carbonate Oil (Gas) Reservoir. Petroleum Industry Press, Beijing, pp. 18–25.
- Jia, L., Cai, C., Jiang, L., Zhang, K., Li, H., Zhang, W., 2016. Petrological and geochemical constraints on diagenesis and deep burial dissolution of the Ordovician carbonate reservoirs in the Tazhong area, Tarim Basin, NW China. *Mar. Petrol. Geol.* 78, 271–290.
- Jiang, Kaixi, He, Wenxiang, Peng, Li, Chen, Zulin, Zhu, Junzhang, Guo, Qingzheng, Xiang, Nian, 2015. Initial exploration mechanism of dissolution of zhujiang carbonates by acid fluids under the burial condition in the liuhua area of the Pearl River Mouth Basin, south China sea. *Bull. China Soc. Mineral Petrol. Geochem.* 34 (3), 592–600.
- Jiang, Z., Chen, D., Qiu, L., Liang, H., Ma, J., 2007. Source-controlled carbonates in a small Eocene half-graben lake basin (Shulu Sag) in central Hebei Province, North China. *Sedimentology* 54 (2), 265–292.
- Jin, Z., Zhu, D., Hu, W., Zhang, X., Zhang, J., Song, Y., 2009. Mesogenetic dissolution of the middle Ordovician limestone in the Tahe oilfield of Tarim basin, NW China. *Mar. Petrol. Geol.* 26 (6), 753–763.
- Kendall, A.C., 1984. Evaporites. In: Walker, R.G. (Ed.), *Facies Models*. Geoscience Canada, pp. 259–296.
- Kong, X., Jiang, Z., Han, C., Zhang, R., 2020. Organic matter enrichment and hydrocarbon accumulation models of the marlstone in the Shulu sag, Bohai Bay Basin, northern China. *Int. J. Coal Geol.* 217, 103350.
- Lambert, L., Durlot, C., Loreau, J.P., Marnier, G., 2006. Burial dissolution of micrite in Middle East carbonate reservoirs (Jurassic–Cretaceous): keys for recognition and timing. *Mar. Petrol. Geol.* 23 (1), 79–92.
- Lao, Qiyuan, Gao, Wenxue, 1984. The characteristics of Cenozoic sedimentary basins in the North China Platform. *Sediment. Geol.* 40 (1–3), 89–103.
- Li, Junwei, 2013. Study Characteristics of the Ancient Buried Hill Carbante Reservoirs in Shulu Depression. Yangtze University, pp. 18–26.
- Li, Qing, 2015. Evaluation of Rudstone and Marlstone Tight Reservoir in Lower Part of the Shahejie 3 Formation of the Shulu Sag, Jizhong Depression. China University of Geosciences, Beijing, pp. 36–38.
- Li, Sanzhong, Suo, Yanhui, Dai, Liming, Liu, Liping, Jin, Chong, Liu, Xin, Tianyao, Hao, Zhou, Lihong, Liu, Baohua, Zhou, Juntao, Qian, Jiao, 2010. Development of the Bohai Bay Basin and destruction of the north China craton. *Earth Sci. Front.* 17 (4), 64–89.

- Liang, Digang, Zeng, Xianzhang, Wang, Xueping, Mou, Luwen, Luo, Qiang, Liu, Baoquan, 2001. Oil and Gas Generation in Jizhong Depression. Petroleum Industry Press, pp. 79–96.
- Liang, Hongbin, Kuang, Hongwei, Liu, Junqi, Guo, Yongjun, Su, Jing, 2007. Discussion on origin for marls of the member 3 of Shahejie Formation of Paleogene in Shulu sag of central heibei depression. *J. Palaeogeogr.* 9 (2), 167–174.
- Liu, Chunyan, Lin, Changsong, Wang, Yi, Wu, Maobing, 2008. Burial Dissolution of Ordovician Granule Limestone in the Tahe Oilfield of the Tarim Basin, NW China, and Its geological significance. *Acta Geologica Sinica* 82 (3), 520–529.
- Liu, C., Xie, Q., Wang, G., He, W., Song, Y., Tang, Y., Wang, Y., 2017. Rare earth element characteristics of the carboniferous Huanglong Formation dolomites in eastern Sichuan Basin, southwest China: implications for origins of dolomitizing and diagenetic fluids. *Mar. Petrol. Geol.* 81, 33–49.
- Longman, M.W., 1980. Carbonate diagenetic textures from nearsurface diagenetic environments. *AAPG Bull.* 64 (4), 461–487.
- Lundegard, P.D., Land, L.S., 1986. Carbon dioxide and organic acids: their role in porosity enhancement and cementation of the Texas Gulf Coast. In: Gautier, D.L. (Ed.), *Roles of Organic Matter in Sediment Diagenesis: SEPM Special Publication* 38, pp. 129–146.
- Machel, H.G., Anderson, J.H., 1989. Pervasive subsurface dolomitization of the nisku Formation in central alberta. *J. Sediment. Res.* 59 (6), 891–911.
- Machel, H.G., Burton, E.A., 1991. Factors governing cathodoluminescence in calcite and dolomite, and their implications for studies of carbonate diagenesis. In: *Luminescence Microscopy and Spectroscopy: Qualitative and Quantitative Applications*. SEPM short course, pp. 37–57.
- Mazzullo, S.J., Harris, P.M., 1991. An Overview of Dissolution Porosity Development in the Deep-Burial Environment, with Examples from Carbonate Reservoirs in the Permian Basin. West Texas Geological Society, Midland, TX, 91–89.
- Mazzullo, S.J., Harris, P.M., 1992. Mesogenetic dissolution: its role in porosity development in carbonate reservoirs. *AAPG Bull.* 76 (5), 607–620.
- Mazzullo, S.J., 2004. Overview of porosity evolution in carbonate reservoirs. *Kansas Geological Society Bulletin* 79 (1–2), 1–19.
- McLennan, S.M., 1989. Rare earth elements in sedimentary rocks: influence of provenance and sedimentary processes. *Geochemistry and Mineralogy of Rare Earth Elements, Reviews in Mineralogy* 21, 169–200.
- Meng, X., Ge, M., Tucker, M.E., 1997. Sequence Sequence stratigraphy, sea-level changes and depositional systems in the Cambro-Ordovician of the North China carbonate platform. *Sediment. Geol.* 114 (1–4), 189–222.
- Möller, P., Bau, M., 1993. Rare-earth patterns with positive cerium anomaly in alkaline waters from Lake Van, Turkey. *Earth Planet Sci. Lett.* 117 (3–4), 671–676.
- Morse, J.W., Mackenzie, F.T., 1990. *Geochemistry of Sedimentary Carbonates*. Elsevier, pp. 511–598.
- Moore, C.H., Wade, W.J., 2013. Carbonate Reservoirs: Porosity and Diagenesis in a Sequence Stratigraphic Framework. Newnes, pp. 59–61.
- Moore, C.H., Druckman, Y., 1981. Burial diagenesis and porosity evolution, upper jurassic smackover, Arkansas and Louisiana. *AAPG (Am. Assoc. Pet. Geol.) Bull.* 65 (4), 597–628.
- Nabelek, P.I., 1987. General equations for modeling fluid/rock interaction using trace elements and isotopes. *Geochem. Cosmochim. Acta* 51 (6), 1765–1769.
- Nesbitt, H.W., 1979. Mobility and fractionation of rare earth elements during weathering of a granodiorite. *Nature* 279 (5710), 206–210.
- Nijenhuis, I.A., Bosch, H.J., Damsté, J.S., Brumsack, H.J., De Lange, G.J., 1999. Organic matter and trace element rich sapropels and black shales: a geochemical comparison. *Earth Planet Sci. Lett.* 169 (3–4), 277–290.
- Qing, H., Mountjoy, E.W., 1994. Rare earth element geochemistry of dolomites in the Middle Devonian Presqu'île barrier, Western Canada Sedimentary Basin: implications for fluid-rock ratios during dolomitization. *Sedimentology* 41 (4), 787–804.
- Ren, C., He, F., Gao, X., Wu, D., Yao, W., Tian, J., Guo, H., Huang, Y., Wang, L., Feng, H., Li, J., 2019. Prediction of exploration targets based on integrated analyses of source rock and simulated hydrocarbon migration direction: a case study from the gentle slope of Shulu Sag, Bohai Bay Basin, northern China. *Geosci. J.* 23 (6), 977–989.
- Rudnick, R.L., Gao, S., 2003. Composition of the continental crust. *The crust* 3, 1–64.
- Sauro, F., Zampieri, D., Filippini, M., 2013. Development of a deep karst system within a transpressional structure of the Dolomites in north-east Italy. *Geomorphology* 184, 51–63.
- Scholle, P.A., Ulmer-Scholle, D.S., 2003. *A Color Guide to the Petrography of Carbonate Rocks: Grains, Textures, Porosity, Diagenesis*. AAPG Memoir 77, vol. 77. AAPG, pp. 352–370.
- Seewald, J.S., 2003. Organic-inorganic interactions in petroleum-producing sedimentary basins. *Nature* 426, 327–333.
- She, Min, Shou, Jianfeng, Shen, Anjiang, Pan, Liyin, Hu, Anping, Hu, Yuanyuan, 2016. Experimental simulation of dissolution law and porosity evolution of carbonate rock. *Petrol. Explor. Dev.* 43 (4), 616–625.
- Surdam, R.C., Crossey, L.J., Hagen, E.S., Heasler, H.P., 1989. Organic-inorganic interactions and sandstone diagenesis. *AAPG (Am. Assoc. Pet. Geol.) Bull.* 73 (1), 1–23.
- Tait, L., 1987. The character of organic matter and the partitioning of trace and rare earth elements in black shales; Blondeau Formation, Chibougamau, Québec. Université du Québec à Chicoutimi. Mémoire. Presente A. 1–494.
- Tan, Fei, Zhang, YunFeng, Wang, ZhenYu, Dong, ZhaoXiong, Huang, ZhengLiang, Wang, QianPing, Gao, JunWei, 2017. Simulation experiment for the burial dissolution of different petrofabric carbonate rocks of ordovician in the Ordos Basin. *Acta Sedimentol. Sin.* 35 (2), 413–424.
- Taylor, H.P., 1974. The application of oxygen and hydrogen isotope studies to problems of hydrothermal alteration and ore deposition. *Econ. Geol.* 69 (6), 843–883.
- Toth, J., 1980. Cross-formational gravity-flow of groundwater: a mechanism of the transport and accumulation of petroleum (the generalized hydraulic theory of petroleum migration). *Problems of Petroleum Migration. Am. Assoc. Pet. Geol. Mem.* 10, 121–169.
- Vacher, H.L., Mylroie, J.E., 2002. Eogenetic karst from the perspective of an equivalent porous medium. *Carbonates Evaporites* 17 (2), 182.
- Valencia, F.L., Laya, J.C., 2020. Deep-burial dissolution in an oligocene-miocene giant carbonate reservoir (perla limestone), gulf of Venezuela basin: implications on microporosity development. *Mar. Petrol. Geol.* 113, 104144.
- Veizer, J., Ala, D., Azmy, K., Bruckschen, P., Buhl, D., Bruhn, F., Carden, G.A., Diener, A., Ebner, S., Godderis, Y., Jasper, T., 1999. $^{87}\text{Sr}/^{86}\text{Sr}$, $\delta^{13}\text{C}$ and $\delta^{18}\text{O}$ evolution of Phanerozoic seawater. *Chem. Geol.* 161 (1–3), 59–88.
- Vine, J.D., Tourtelot, E.B., 1970. Geochemistry of black shale deposits; a summary report. *Econ. Geol.* 65 (3), 253–272.
- Wierzbicki, R., Dravis, J.J., Al-Aasm, I., Harland, N., 2006. Burial dolomitization and dissolution of upper Jurassic Abenaki platform carbonates, deep Panuke reservoir, Nova Scotia, Canada. *AAPG Bull.* 90 (11), 1843–1861.
- Wright, P., Harris, P.M., 2013. Carbonate dissolution and porosity development in the burial (mesogenetic) environment. In: *AAPG Annual Convention and Exhibition, Search and Discovery*. Article #50860, Pittsburgh, PA, pp. 19–22.
- Xiang, P., Ji, H., Shi, Y., Huang, Y., Sun, Y., Xu, X., Zou, S., 2020. Petrographic, rare earth elements and isotope constraints on the dolomite origin of Ordovician Majiagou Formation (Jizhong Depression, North China). *Mar. Petrol. Geol.* 104374.
- Xu, S., Bi, H., Li, S., Somerville, I., Ye, Q., Feng, H., Li, M., 2017. Deep burial dissolution of lower palaeozoic carbonates and the role of compacted released water from palaeogene strata in the zhuanghai area, jiyang depression, Bohai Bay Basin, NE China. *Geol. J.* 52 (1), 30–44.
- Zhao, Guoxiang, Wang, Qingbin, Yang, Bo, Wang, Xiaogang, Bai, Bing, Lin, Wan, 2016. Dissolution mechanism analysis of Ordovician carbonates under burial environment of Bozhong Sag, Bohai Sea area. *Natural Gas Geoscience* 27 (1), 111–120.
- Zhao, Xianzheng, Zhu, Jieqiong, Zhang, Ruifeng, Yu, Zhanwen, Wang, Jimao, Guo, Yongjun, 2014. Characteristics and exploration potential of tight calcilutite-rudstone reservoirs in Shulu sag, Jizhong depression, North China. *ACTA PETROLEI SINICA* 35 (4), 613–622.
- Zhu, Dongya, Hu, Wenxuan, Zhang, Xuefeng, Zhijun, J., 2007. Characteristics of burial dissolution in the ordovician limestone of tahe oilfield. *Acta Pet. Sin.* 28 (5), 57–62.
- Zou, Xianhua, Chen, Jiangyi, Wen, Da, 2015. The regularity and distribution of hydrocarbon accumulation in buried hills of Shulu Sag. *Journal of Yangtze University (Natural Science Edition)* 12 (5), 19–22.